Molecular Therapy
Nucleic Acids
Original Article

RAB18 regulates extrahepatic siRNA-mediated gene silencing efficacy

Jiamiao Lu,[1] Jasper Lee,[1] Eric Yuan,[1] Devin L. Wakefield,[1] Matt Kanke,[1] Danielle Pruitt,[2] Jose Barreda,[2] Ingrid C. Rulifson,[2] Jiansong Xie,[1] John Ferbas,[1] Jason Long,[3] Bryan Meade,[3] Oliver Homann,[4] Wei Guo,[2] Tina Gomes,[1] Hong Zhou,[1] Bin Wu,[5] Jixin Cui,[2] and Songli Wang[1]

[1]Precision Biology, Amgen Inc., South San Francisco, CA 94080, USA; [2]Cardiometabolic Disorders, Amgen Inc., South San Francisco, CA 94080, USA; [3]RNA Therapeutics, Amgen Inc., Thousand Oaks, CA 91320, USA; [4]CRADI Computational Biology, Amgen Inc., South San Francisco, CA 94080, USA; [5]Therapeutic Discovery, Amgen Inc., Thousand Oaks, CA 91320, USA

Small interfering RNAs (siRNAs) hold considerable therapeutic potential to selectively silence previously "undruggable" disease-associated targets, offering new opportunities to fight human diseases. This therapeutic strategy, however, is limited by the inability of naked siRNAs to passively diffuse across cellular membranes due to their large molecular size and negative charge. Delivery of siRNAs to liver through conjugation of siRNA to N-acetylgalactosamine (GalNAc) has been a success, providing robust and durable gene knockdown, specifically in hepatocytes. However, the poor delivery and silencing efficacy of siRNAs in other cell types has hindered their applications outside the liver. We previously reported that a genome-wide pooled knockout screen identified *RAB18* as a major modulator of GalNAc-siRNA conjugates. Herein, we demonstrate *RAB18* knockout/knockdown efficaciously enhances siRNA-mediated gene silencing in hepatic and extrahepatic cell lines and *in vivo*. Our results reveal a mechanism by which retrograde Golgi-endoplasmic reticulum (ER) transport and the intracellular lipid droplets (LDs) positively regulate siRNA-mediated gene silencing.

INTRODUCTION

During the last decade, clinical success of small interfering RNA (siRNA)-based medicines transformed the drug development pipeline; targets once considered undruggable are now druggable using high-specificity siRNA technology. siRNAs exert their effect through RNA interference (RNAi) of targeted mRNAs. Despite the remarkable success of delivering therapeutic siRNAs specifically to hepatocytes through GalNAc conjugation, delivery of efficacious amounts of siRNA to extrahepatic cells or tissues with specificity, potency, and durability remains challenging. To extend our mechanistic understanding of how intracellular siRNA-mediated gene silencing is regulated, we previously conducted a genome-wide pooled CRISPR-Cas9 screen based on the delivery of GalNAc-conjugated siRNA targeting the *HPRT1* gene in the human hepatocellular carcinoma line Hep3B.[1] This screen identified multiple candidate genes that, when knocked out, enhanced siRNA-mediated gene silencing in Hep3B cells. One of the top candidate genes identified through this screen was *RAB18*. To elucidate the impact of *RAB18* on siRNA-mediated gene silencing, we generated *RAB18*-knockout and -overexpression Hep3B cells. Our previous data indicate that depletion of *RAB18* improves siRNA-mediated gene silencing for siRNAs delivered by conjugation to GalNAc, cholesterol, or anti-ASGR1 antibodies, but not via liposome-mediated transfection. Here, we extend our previous findings from hepatic cells to extrahepatic cells and demonstrate translation of the *in vitro* results to an *in vivo* mouse model. In a standard GalNAc-siRNA conjugate trafficking event, the GalNAc-siRNA molecules are internalized into hepatocytes through asialoglycoprotein receptor (ASGPR)-mediated endocytosis. As endosomes mature, the internal pH decreases, resulting in the release of the GalNAc-siRNA molecules from ASGPRs. Subsequently, ASGPRs recycle back to the cell surface while GalNAc-conjugated siRNAs remain inside the endosomes.[2] GalNAc and the linkers are subsequently degraded while a small fraction of the remaining free siRNAs (<1%) are released from the endosomes. Once in the cytoplasm, the siRNA molecules access RNA-induced silencing complex (RISC), resulting in target transcript degradation and inhibited protein translation.[2,3] Liposome transfection-mediated siRNA delivery induces mRNA knockdown at low siRNA concentrations, possibly due to the ability of liposome-containing vesicles to perform random Brownian motion within the cytoplasm to help siRNA circumvent some of the intracellular barriers encountered by alternative delivery methods such as GalNAc, cholesterol, or antibody-mediated uptake.[4] Previously we observed that the activity of siRNA delivered by liposomes was not altered by *RAB18* knockout; thus, we deduced *RAB18* specifically regulates the silencing effect of siRNA delivered through ligand-conjugated methods.[1] The protein encoded by the *RAB18* gene is a member of RAS-related small GTPases that regulate membrane trafficking in organelles and transport vesicles. Studies link *RAB18* to the regulation of lipid droplet (LD) formation,[5,6]

Received 6 May 2024; accepted 5 September 2024;
https://doi.org/10.1016/j.omtn.2024.102335.

Correspondence: Jiamiao Lu, PhD, Precision Biology, Amgen Inc., South San Francisco, CA 94080, USA.
E-mail: jlu01@amgen.com
Correspondence: Songli Wang, PhD, Precision Biology, Amgen Inc., South San Francisco, CA 94080, USA.
E-mail: songliw@amgen.com

inhibition of COPI-independent retrograde trafficking from Golgi to endoplasmic reticulum (ER),[7] regulation of secretory granules[8] and peroxisomes,[9] promotion of hepatitis C virus (HCV) assembly on the LD membrane,[10] and regulation of ER structure.[11] To elucidate the mechanism responsible for the effect of *RAB18* knockout on siRNA-mediated gene silencing, we conducted a series of experiments to demonstrate that retrograde Golgi-ER transport and LDs positively regulate siRNA-mediated gene silencing.

RESULTS

RAB18 gene expression negatively correlates with both siRNA- and antisense oligonucleotide-mediated gene silencing

In previous studies, we demonstrated *RAB18* knockout/knockdown enhances the silencing effect of siRNAs delivered by GalNAc, cholesterol, or antibodies, but not siRNAs delivered by liposome-mediated transfection in Hep3B cells by using siRNA targeting *HPRT1*, *PPIB*, and *ASGR1* genes.[1] To better understand the correlation between *RAB18* gene expression and siRNA activity, we opted to use an siRNA targeting the *HPRT1* gene for further study. We generated *RAB18*-overexpressing Hep3B cells. Both the previously validated Cas9 stable Hep3B cells (Hep3BCas9) and the corresponding *RAB18*-knockout Hep3BCas9 cells (Hep3BRAB18KO)[1] were transduced with lentivirus expressing a *RAB18*-overexpression construct (Figure S1A). The mCherry-positive populations were sorted for *RAB18*-overexpressing cells, Hep3BCas9RAB18_OE and Hep3BRAB18KO_OE (Figures 1A and 1B), and *RAB18* overexpression was confirmed by digital polymerase chain reaction (dPCR) (Figures S1B and S1C). Next, the *HPRT1* gene expression level was measured in Hep3BCas9, Hep3BRAB18KO, Hep3BCas9RAB18_OE, and Hep3BRAB18KO_OE cells treated with either GalNAc-conjugated siRNA targeting the *HPRT1* gene (GalNAc-*HPRT1* siRNA, compound no. 8172, human-mouse cross reactive) or the control GalNAc-conjugated siRNA target a housekeeping gene, *PPIB*, as a negative control for *HPRT1* gene silencing (GalNAc-*PPIB* siRNA, compound no. 8714) (Table S1). Hep3BRAB18KO cells demonstrated enhanced *HPRT1* siRNA silencing efficacy (half maximal inhibitory concentration [IC50] = 2.69 nM), while overexpression of *RAB18* in Hep3BRAB18KO cells mitigated *HPRT1* siRNA silencing efficacy (IC50 = 19.25 nM) (Figure 1B); a similar pattern was observed when *RAB18* was overexpressed in Hep3BCas9 cells (Figure 1A). Thus, these data demonstrate *RAB18* gene expression negatively correlates with siRNA-mediated gene silencing.

To determine if *RAB18* regulates the silencing efficacy of single-stranded antisense oligonucleotides (ASOs), we performed a set of similar experiments. Hep3BCas9 parental cells and Hep3BRAB18KO cells were treated with either PBS or increasing concentrations of one of two GalNAc-conjugated ASO molecules targeting the *HPRT1* gene (compound nos. 15469 and 15470). Sequences for each of the three GalNAc-conjugated ASO molecules are described in Table S2. As demonstrated in Figure 1C, after 4 days, Hep3BRAB18KO cells treated with GalNAc-conjugated ASO molecules targeting *HPRT1* resulted in enhanced silencing of *HPRT1* compared to Hep3BCas9 cells receiving the same ASO (Figure 1C). For example, the IC50 value for compound no. 15469 in Hep3BCas9 parental cells was 242.6 nM, whereas the IC50 value for the same compound in Hep3BRAB18KO cells was 12.58 nM, a 20-fold enhancement of silencing efficacy. These results suggest that *RAB18* regulates an intracellular step similarly used by both GalNAc-conjugated siRNA molecules and GalNAc-conjugated ASO molecules.

RAB18 knockout enhances siRNA-mediated gene silencing in extrahepatic cells

Since the *RAB18* gene is expressed ubiquitously in mammalian tissues, we next addressed the effect of *RAB18* expression on siRNA-mediated gene silencing in extrahepatic cells. Based on our internal RNA sequencing (RNA-seq) data (Table S3), *RAB18* gene expression is lower in hepatic Hep3B cells compared to the breast cancer cell line T47D (Table S3). Thus, we initiated confirmation of *RAB18* function on regulating siRNA-mediated gene silencing in extrahepatic T47D cells. To generate *RAB18*-knockout T47D cells, we co-delivered lentivirus packaging Cas9 (blasticidin resistant) with lentivirus packaging guide RNA (gRNA) targeting the *RAB18* gene (puromycin resistant) (SIGMA vector: U6-gRNA: PGK-puro-2A-tagBFP) into T47D cells. The T47D *RAB18*-knockout cells (T47DRAB18KO) were enriched by blasticidin and puromycin selection. In parallel, Cas9 stable T47D control cells (T47DCas9) were generated by transducing lentivirus packaging Cas9. Inference of CRISPR edit (ICE) analysis confirmed successful knockout of the *RAB18* gene (Figure S2A) with no effect on cell viability (Figure S2B). Both negatively charged and large, unconjugated siRNA molecules do not easily enter cells without conjugation. However, trace amounts of siRNA could be engulfed by cells via pinocytosis.[12] To evaluate the possibility of pinocytosis, unconjugated *HPRT1* siRNA (compound no. 39986; Table S1) was added to T47D cells. Despite sub-optimal delivery, unconjugated *HPRT1* siRNA led to robust target gene silencing in both T47DRAB18KO and Hep3BRAB18KO cells, but not in the parental T47DCas9 and Hep3BCas9 cells (Figure 2A), demonstrating *RAB18* serves as a roadblock in siRNA-mediated gene silencing in both hepatic and extrahepatic cells.

To determine if the regulatory role of *RAB18* translates across other extrahepatic cell types, additional extrahepatic cell lines with varying levels of *RAB18* expression were selected to generate *RAB18* knockouts. These cell lines include pancreatic cancer cell line MiaPaCa-2, kidney cancer cell line A498, lung cancer cell line NCIH1299, colorectal cancer cell lines COLO205 and HT-29, and breast cancer cell line MCF7 (Table S3). To simplify the production of *RAB18*-deficient cells, Cas9 protein and three synthesized sgRNAs (single guide RNA) targeting *RAB18* gene (Table S4) were electroporated into the cell lines. Cells electroporated with only Cas9 protein were used as controls. The effect of *RAB18* ablation was evaluated by ICE analysis and western blot (Figures 2B and 2C). The validated *RAB18* knockouts and their Cas9 control cells were subsequently treated with unconjugated *HPRT1* siRNA. As summarized in Figures 2D and 2E, *RAB18* ablation robustly enhanced siRNA-mediated gene silencing of unconjugated *HPRT1* siRNA in MiaPaCa-2 cells and moderately

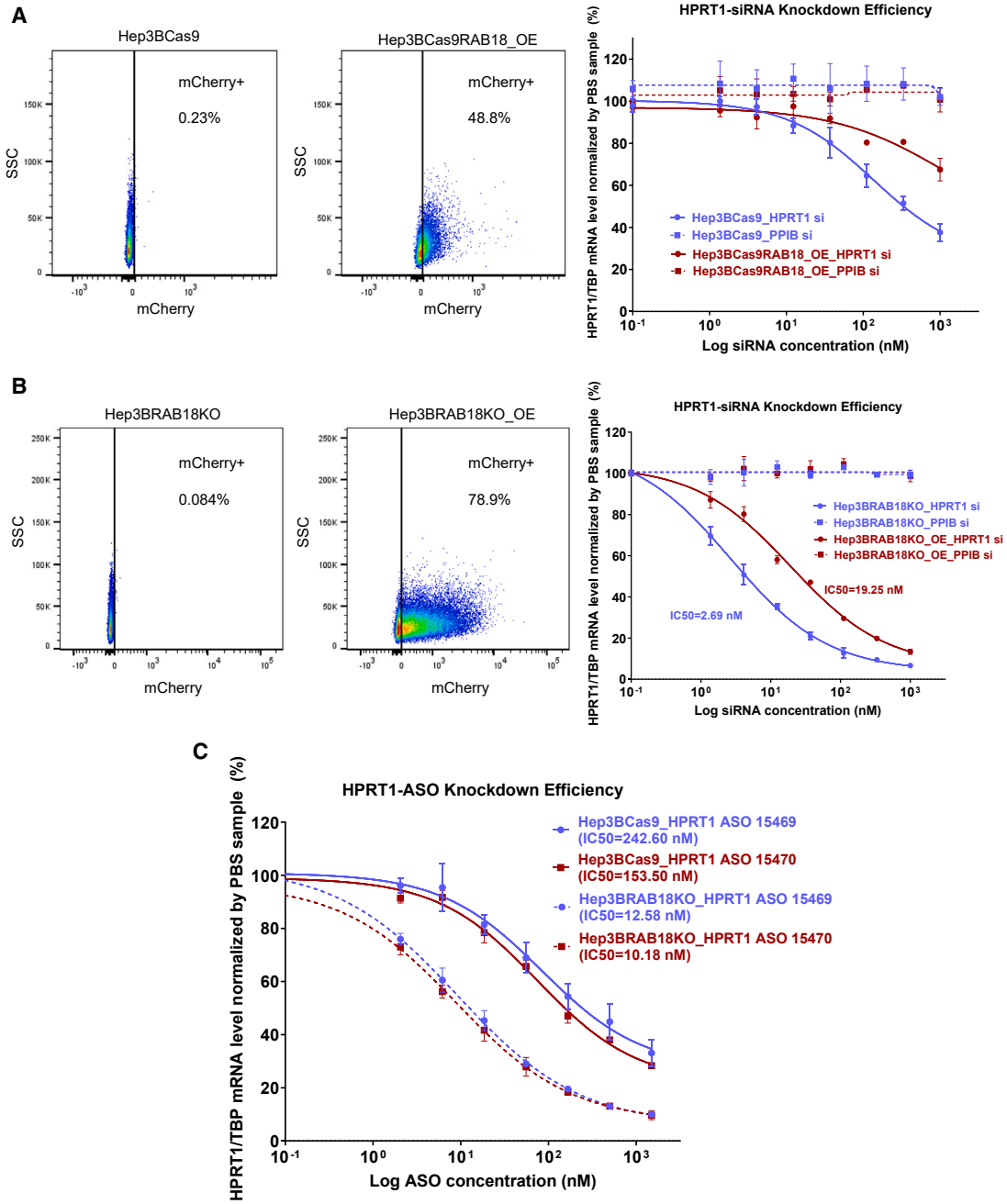

Figure 1. Impact of *RAB18* gene expression on the silencing efficacy of siRNA and ASO molecules

(A) Effect of *RAB18* overexpression on siRNA-mediated gene silencing in Hep3BCas9 cells. The left and middle figures show flow cytometry data demonstrating the successful overexpression of the *RAB18* gene using a lentivirus vector (Figure S1A). Cells overexpressing *RAB18* are mCherry positive. The figure on the right shows dPCR measurements of *HPRT1* expression in GalNAc-*HPRT1* siRNA-treated Hep3BCas9 cells and Hep3BCas9RAB18_OE cells (n = 3). (B) Effect of *RAB18* overexpression on siRNA-mediated gene silencing in Hep3BRABKO cells. The left and middle figures show the flow cytometry data, which demonstrate the successful overexpression of the *RAB18* gene in Hep3BRAB18KO cells. The right figure shows dPCR measurements of *HPRT1* expression in GalNAc-*HPRT1* siRNA-treated Hep3BRAB18KO cells and the *RAB18*-overexpression Hep3BRAB18KO_OE cells (n = 3). (C) dPCR measurements of *HPRT1* expression in Hep3BCas9 and Hep3BRAB18KO cells treated with GalNAc-conjugated ASO molecules targeting the *HPRT1* gene (15469, 15470) (n = 3). All samples were measured 4 days post siRNA treatments. All dPCR results were normalized by the control housekeeping gene, *TBP*, and no siRNA (PBS only)-treated control groups. All error bars represent standard deviation (SD).

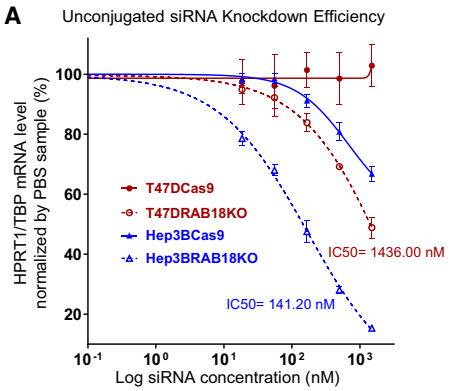

B

Editing score on RAB18 gene assessed by ICE analysis

Cell line	ICE Score (%)	KO Score (%)
MiaPaCa-2 RAB18KO	100	96
A498 RAB18KO	100	99
NCIH1299 RAB18KO	100	98
COLO205 RAB18KO	88	88
HT29 RAB18KO	100	99
MCF7 RAB18KO	100	100

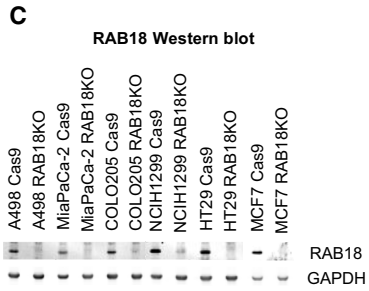

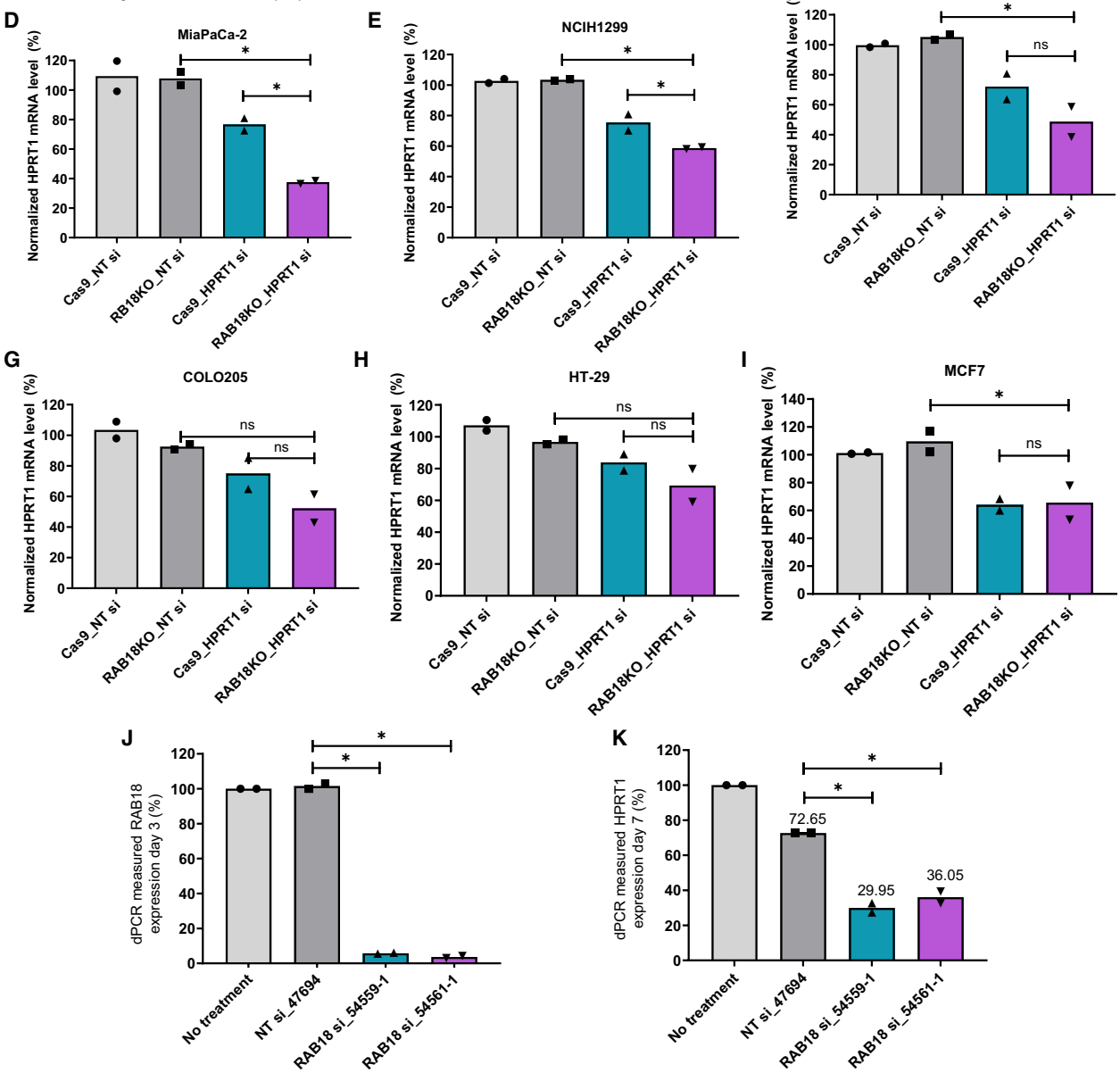

(legend on next page)

in NCIH1299 cells. No overt effect was observed in the A498, COLO205, HT-29, and MCF7 *RAB18*-deficient cell lines (Figures 2F–2I). The internalization rate of unconjugated *HPRT1* siRNA may depend on the rate of pinocytosis, and thus the robustness of siRNA-mediated silencing could vary across cells due to differing levels of pinocytosis.

When validating siRNA silencing effect in immortalized cell lines, it is possible that the effect of internalized siRNA is diluted rapidly by cell division limiting the degree of gene silencing. To retain the intracellular effect of siRNA, the impact of *RAB18* on siRNA-mediated gene silencing in extrahepatic cells was evaluated in non-proliferating human iPSC-derived cardiomyocytes. Using liposome-mediated transfection, two different unconjugated *RAB18* siRNAs (54559-1 and 54561-1) resulted in *RAB18* mRNA knockdown by day 3 post transfection while non-targeting (NT) siRNA had no effect (Figure 2J). After washing and replacing medium, the cells were then treated with unconjugated siRNA targeting the *HPRT1* gene for an additional 4 days. As shown in Figure 2K, after treatment with *HPRT1* siRNA, *HPRT1* mRNA expression level was at 29.95% or 36.05%, respectively, in cells pre-treated with one of two different *RAB18* siRNAs compared to 72.65% in the cells pre-treated with NT siRNA. These results further demonstrate the regulatory role *RAB18* expression has on siRNA-mediated gene silencing in extrahepatic cells.

Knocking down *Rab18* in mouse liver enhances the target gene silencing effect of GalNAc-*HPRT1* siRNA

We have thus far demonstrated enhanced siRNA-mediated gene silencing in multiple hepatic and extrahepatic cell lines by generating *RAB18* knockout or knockdown *in vitro*. To explore translatability, we next evaluated the effect of localized *RAB18* deletion *in vivo*. Global, germline *RAB18* deficiency leads to inherited human disease, Warburg micro syndrome. Although no significant dysfunction or toxicity was observed in *RAB18*-knockout immortalized cell lines or human iPSC-derived cardiomyocytes, we were concerned about the potential of global deficiency *in vivo*. Therefore, instead of using *Rab18*-deficient mice that have been reported to exhibit major ocular and neurological abnormalities associated with Warburg micro syndrome,[13] we used *Rab18* siRNA to temporally knockdown *Rab18* in mouse liver to study its impact on siRNA activity *in vivo*. To prepare for *in vivo* testing, we designed and validated 26 human-mouse cross-reactive siRNA molecules targeting the *RAB18*/*Rab18* gene in human Hep3B and mouse Hepa 1–6 cells through liposome-mediated transfection (Tables S5 and S6). The off-target potential of the six most potent *RAB18* siRNA triggers (54559-1, 54561-1, 54570-1, 54564-1, 54569-1, and 54553-1) was predicted based on near-perfect complementarity (data not shown). Bioinformatic analysis identified triggers 54561-1, 54570-1, 54564-1, and 54553-1 with the least off-target potential. These triggers were then conjugated with GalNAc for *in vivo* studies (Table S7). The siRNA-mediated gene silencing effect of these GalNAc-conjugated *Rab18* triggers (64131-1, 64134-1, 64137-1, and 64140-1) along with the negative control GalNAc-conjugated NT siRNA (42105-3) and positive control GalNAc-conjugated siRNA targeting *Hprt1* gene (8172) were evaluated in mouse livers. As outlined in Figure 3A, 2 weeks after subcutaneous (s.c.) injection of siRNAs, mouse livers were collected for RNA isolation, and the mRNA levels of *Rab18* and *Hprt1* were determined by dPCR. As expected, *Hprt1* siRNA established more than 80% silencing of the *Hprt1* gene on day 14 post injection; no impact on *Rab18* mRNA expression was detected (Figures 3B and 3C) and no change in either *Hprt1* or *Rab18* mRNA was detected in animals injected with vehicle (PBS) or NT siRNA (Figures 3B and 3C). *Rab18* mRNA knockdown was achieved by all *Rab18* siRNAs assessed; 64131-1 established the most robust silencing of *Rab18* mRNA (88%) without altering *Hprt1* mRNA (Figures 3B and 3C). No notable impact on body weight (Figure S3A) or serum liver transaminase levels (Figures S3B–S3D) were detected among the molecules except with 64137-1, indicating potential issues with this siRNA molecule.

To evaluate the global transcriptomic impact of *Rab18* knockdown in the mice, RNA-seq analysis was performed on RNA extracted from all livers. Comparison of the vehicle injection group with the NT or the *Hprt1*-positive control groups showed minor transcriptional changes (Figures S4A and S4B). *Rab18* siRNA treatment, however, elicited a much stronger transcriptomic response (Figures 3D, 3E, and S4C). The data revealed more transcriptomic changes in samples treated with *Rab18* siRNA triggers. However, the level of response did not correlate with the degree of *Rab18* knockdown, indicating trigger-sequence-specific contributions in addition to *Rab18* gene function-related changes. We focused on *Rab18* siRNA, 64131-1, as the severity of *Rab18* knockdown was greatest with this trigger and represents the best candidate to identify *Rab18*-mediated responses. Differential expression analysis revealed a strong bi-directional transcriptomic response, with *Rab18* as the most significantly downregulated gene (Figure 3E). Pathway analysis of upregulated genes revealed processes related to lipid/cholesterol metabolism and downregulated genes revealed processes related to cell cycle (Figures 3F and 3G). A similar pathway analysis using upregulated genes from the NT siRNA

Figure 2. Impact of *RAB18* knockout on siRNA-mediated gene silencing in extrahepatic cells

(A) dPCR measurements of *HPRT1* expression in Hep3BCas9, Hep3BRAB18KO, T47DCas9, and T47DRAB18KO cells treated with unconjugated *HPRT1* siRNA (39986) ($n = 4$). (B) Editing efficacy on the *RAB18* gene assessed by ICE analysis. (C) Editing efficacy on the *RAB18* gene analyzed by western blot of extrahepatic cell lines. (D–I) dPCR measurements of *HPRT1* expression in *RAB18*-knockout extrahepatic cell lines and their control cell lines (Cas9 only) treated with unconjugated *HPRT1* siRNA or unconjugated non-targeting (NT) siRNA. All samples were measured 4 days post siRNA treatments. All dPCR results shown were normalized by *TBP* and no-siRNA (PBS only)-treated control groups. (J) dPCR measurements of *RAB18* gene expression 3 days post *RAB18* siRNA and NT siRNA transfection in human iPSC-derived cardiomyocytes. (K) dPCR measurements of *HPRT1* gene expression of human iPSC-derived cardiomyocytes transfected with *RAB18* siRNA or NT siRNA followed by treatment of GalNAc-*HPRT1* siRNA (7 days post *RAB18* siRNA and NT siRNA transfection). Asterisk indicates significant difference (*$p < 0.05$); ns, not significant based on one-way ANOVA test. All error bars represent SD.

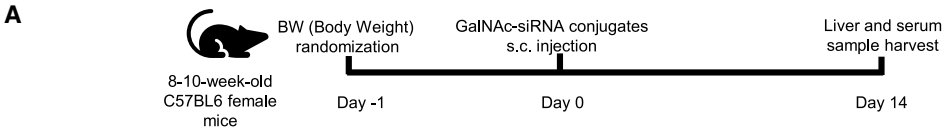

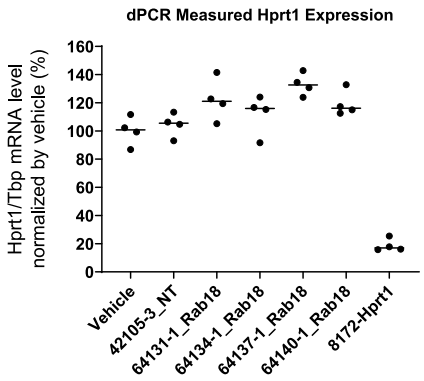

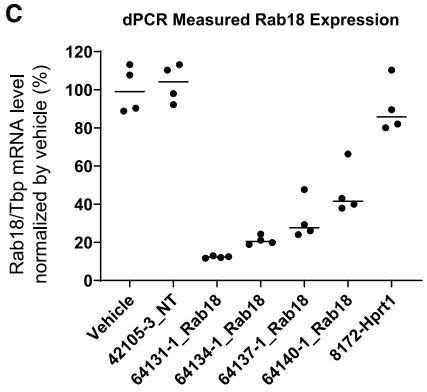

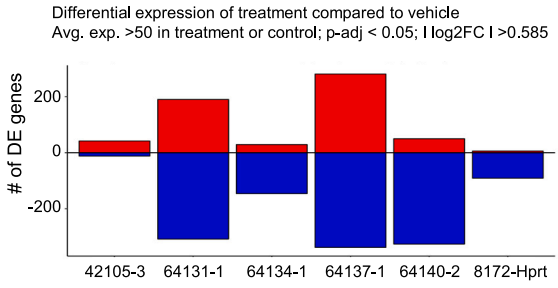

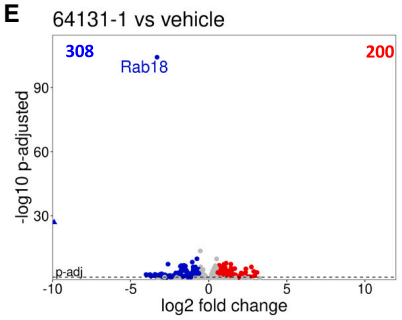

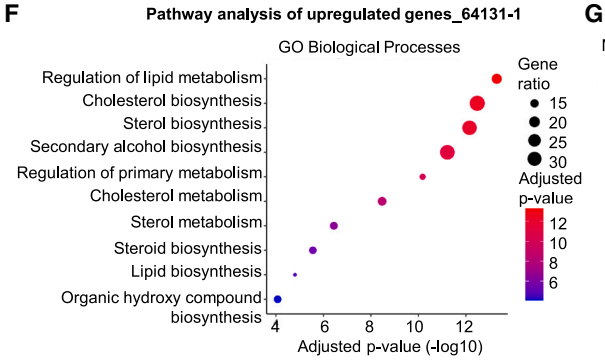

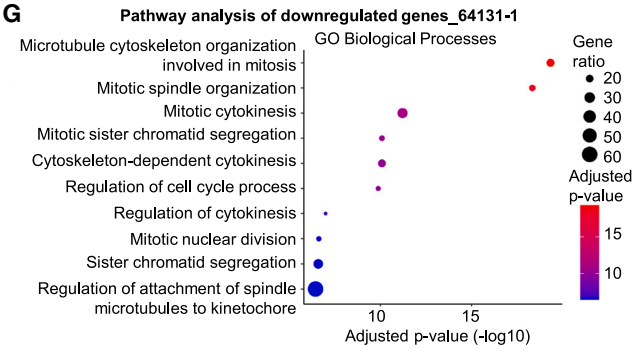

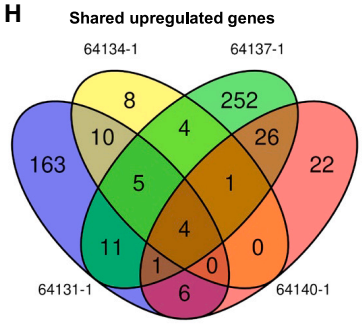

Shared upregulated genes
Nr1d2
2210418010Rik
Upp2
Gm19680

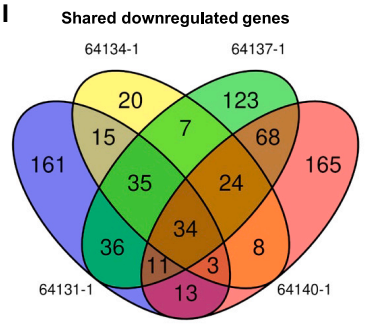

Shared downregulated genes			
Kif20a	Incenp	Kpna2-ps	Icam1
Abcg1	Ccdc120	Sirpa	Ccnb2
Adgre1	Kif23	Rab18	Anln
Arhgap19	Plk1	Siglece	Gm20342
Kif4	Cenpe	Cdca3	Pou2f2
Depdc1a	Aspm	Rassf4	Gm48309
Kif2c	Knstrn	C3ar1	Btbd11
Kif18b	Aurka	Ckap2	
Spdl1	Arhgap11a	Gtse1	

(legend continued on next page)

(42105-3)-treated samples did not recapitulate the 64131-1 results, indicating the differentially expressed genes identified in 64131-1-treated samples are not related to general siRNA treatment (Figure S4D). *Rab18* siRNA, 64137-1, was less effective at inducing mRNA knockdown than 64131-1 or 64134-1 yet elicited the strongest overall transcriptomic response compared to vehicle (Figures 3D and S4C). Pathway analysis of upregulated genes revealed 64137-1 treatment altered mitochondrial function related to drug-induced liver injury (DILI), which could indicate potential toxicity issues of this trigger; this was further supported by serum liver transaminase levels (Figures S3B, S3D, and S4E). Few upregulated genes were shared across all four *Rab18* siRNA triggers. Of the four shared upregulated genes, *Nr1d2* is known to play a role in carbohydrate and lipid metabolism (Figure 3H). Pathway enrichment analysis of the 34 shared downregulated genes across all four *Rab18* siRNA triggers highlights an effect on the cell cycle (Figure 3I). Furthermore, several kinesins are present on the list, which may indicate loss of transport of cellular cargo (Figure 3I). By analyzing ~1,400 liver-toxicity-associated genes, no marked change in expression was observed (Figures S4F and S4G).

Because the most potent *Rab18* siRNA, 64131-1, did not induce indications of cell toxicity, it was selected for an *in vivo* study to evaluate if reducing *Rab18* expression could enhance siRNA-mediated gene silencing. As illustrated in Figure 4A, mice were subjected to sequential subcutaneous administration of GalNAc-conjugated siRNAs, or vehicle, as indicated. On day 0, either PBS (vehicle) or 3 mg/kg NT siRNA was administered to control groups (1 and 4–8) and 3 mg/kg *Rab18* siRNA 64131-1 was injected in treatment groups (2–3) to knockdown *Rab18* expression. On day 14, each animal received either a second injection of PBS (groups 1, 3, and 5) or a second injection of *Hprt1* siRNA (8172) at different dosages (0.5 mg/kg [groups 2, 4, and 6], 1 mg/kg [group 7], or 3 mg/kg [group 8]). On day 28, body weights were recorded (Figure S5A) and serum collected for liver transaminases (Figures S5B–S5D). Livers were harvested, RNA isolated, and *Rab18* and *Hprt1* mRNA expression levels were assessed by dPCR. *Rab18* expression was reduced more than 80% in *Rab18* siRNA-treated animals (Figure 4B). The effect of *Rab18* on *Hprt1* expression data is summarized in Figure 4C. In negative control groups (1, 3, and 5), injection with either vehicle, *Rab18* siRNA, or NT siRNA followed by a second injection of vehicle did not reduce *Hprt1* mRNA expression. For positive control groups (group 4), in which animals received 0.5 mg/kg *Hprt1* siRNA following NT siRNA, *Hprt1* mRNA expression was 79.71%. In contrast, *Hprt1* mRNA expression in group 2, in which animals received 0.5 mg/kg *Hprt1* siRNA following 3-mg/kg *Rab18* siRNA injection, was 51.00% of control, which is similar to the level of *Hprt1* detected group 7, in which animals received 1 mg/kg *Hprt1* siRNA following vehicle injection. These results provide translational *in vivo* evidence that *Rab18* negatively regulates siRNA-mediated gene silencing.

RAB18 knockout correlates with reduced intracellular siRNA over time

In a previous study, the effect of *RAB18* on siRNA internalization was evaluated in Hep3BCas9 and Hep3BRAB18KO cells.[1] Briefly, cells were treated with fluorescently labeled GalNAc-conjugated *HPRT1* siRNA for 0.5, 2, 4, and 20 h and then the internalization of siRNA molecules was assessed by flow cytometry. Using this assay, we observed no notable change in the amount of internalization between Hep3BCas9 and Hep3BRAB18KO cells.[1] To study the dynamics of intracellular siRNAs further, we repeated the assay by incubating cells with GalNAc-conjugated *HPRT1* siRNA for 6 h, 1 day, or 2 days, and then used an imaging-based assay and rabbit polyclonal anti-siRNA antibody recognizing 2′OMe- and 2′F-containing oligonucleotides to quantitate the number of intracellular siRNA molecules. As summarized in Figure 5A, after 6 h of siRNA treatment, the intracellular siRNA counts were similar for Hep3BCas9 (17.64/cell) and Hep3 BRAB18KO (15.53/cell) cells. However, as the siRNA treatment extended, fewer siRNA molecules accumulated in the Hep3BRAB18KO (23.47/cell on day 2) cells versus the Hep3BCas9 (31.00/cell on day 2) cells. Thus, although *RAB18* knockout appeared to have no impact on siRNA internalization in this system, it might reduce the accumulation of siRNAs or increase the consumption, or degradation, of siRNA.

Retrograde transport positively regulates siRNA-mediated gene silencing

A previously published study showed *RAB18* mutants enhance retrograde Golgi-ER transport of the COPI-independent cargo.[7] To study the biological mechanisms behind enhanced siRNA-mediated gene silencing in *RAB18*-knockout cells, we investigated whether retrograde Golgi-ER transport regulates siRNA-mediated gene silencing. Golgicide A (GCA) is a powerful Golgi inhibitor that can specifically inhibit assembly of COPI-coated vesicles and lead to inhibition of COPI-dependent retrograde Golgi-ER transport.[14,15] As illustrated in Figure 5B, *RAB18* inhibits COPI-independent retrograde transport and GCA treatment inhibits COPI-dependent retrograde transport. If

Figure 3. Results from the *in vivo* study evaluating the silencing effect of GalNAc-*Rab18* siRNA triggers and transcriptomic analysis of liver RNA samples harvested from siRNA-treated mice

(A) Schematic diagram illustrating the experimental workflow for the *in vivo* study. (B) dPCR measurements of *Hprt1* expression in liver RNA samples harvested 14 days post -s.c. injection. (C) dPCR measurements of *Rab18* expression in liver RNA samples harvested 14 days post s.c. injection. All dPCR results were normalized by *Tbp* and the control vehicle (PBS)-treated control groups. (D) Number of significant differentially expressed genes across all experimental groups as compared to vehicle control. Genes with a *p*-adjusted <0.05 and a fold-change >1.5 (up) or < −1.5 (down) were considered significantly differentially expressed for all panels. (E) Volcano plot of differentially expressed genes in 64131-1-treated samples compared with vehicle-treated control group. The numbers of significantly downregulated (blue) or upregulated - (red) genes are indicated at the top. (F) Top enriched Gene Ontology (GO) biological processes gene sets among upregulated genes from (E). (G) Top enriched GO biological processes gene sets among downregulated genes from (E). (H) Venn diagram and list of shared upregulated genes identified in all *Rab18* siRNA trigger-treated samples compared to vehicle control. (I) Venn diagram and list of shared downregulated genes identified in all *Rab18* siRNA trigger-treated samples compared to vehicle control. The adjusted *p*-value is calculated using the Benjamini-Hochberg method.

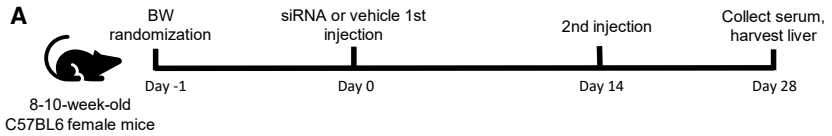

	Day 0 injections		Day 14 injections		Day 28
Group Number	GalNAc-siRNA Conjugates	Dose (mg/kg)	GalNAc-siRNA Conjugates	Dose (mg/kg)	
1	Vehicle	NA	Vehicle	NA	Harvest
2	64131-1_RAB18 si	3	8172_HPRT si	0.5	Harvest
3	64131-1_RAB18 si	3	Vehicle	NA	Harvest
4	42105-3_NT si	3	8172_HPRT si	0.5	Harvest
5	42105-3_NT si	3	Vehicle	NA	Harvest
6	Vehicle	NA	8172_HPRT si	0.5	Harvest
7	Vehicle	NA	8172_HPRT si	1	Harvest
8	vehicle	NA	8172_HPRT si	3	Harvest

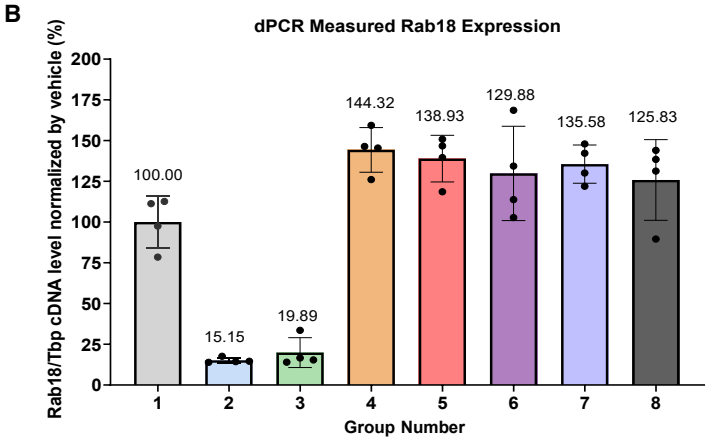

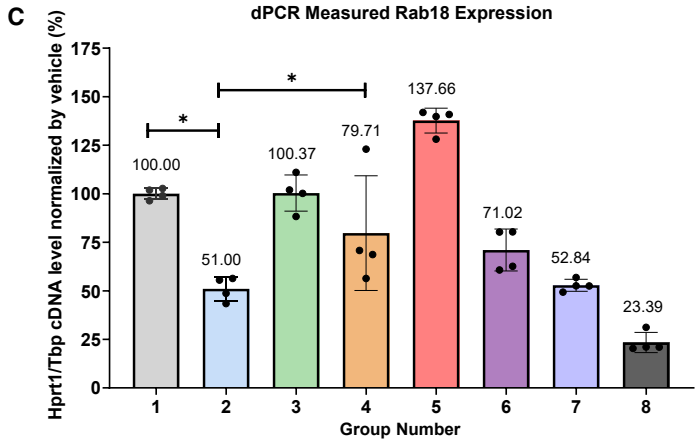

Figure 4. Results from the second *in vivo* study evaluating the effect of *Rab18* knockdown on siRNA-mediated gene silencing

(A) Schematic diagram illustrating the experimental workflow and group design for the second *in vivo* study. (B) dPCR measurements of *Rab18* expression in liver RNA samples harvested 28 days post s.c. injection. (C) dPCR measurements of *Hprt1* expression in liver RNA samples harvested 28 days post s.c. injection. All dPCR results were normalized by *Tbp* and the control vehicle (PBS)-treated control groups. Asterisk indicates significant difference (*$p < 0.05$) based on one-way ANOVA test. All error bars represent SD.

retrograde transport positively regulates siRNA function, siRNA conjugates should exhibit the weakest silencing effect of the target gene in Hep3BCas9 cells treated with GCA (group 2). Conversely, siRNA conjugates should exert the strongest silencing of the target gene in Hep3BRAB18KO cells and without GCA treatment (group 3), since both COPI-independent and COPI-dependent retrograde transport pathways are unobstructed under this condition. To test this hypothesis, siRNA-mediated gene silencing of GalNAc-*HPRT1* siRNA was validated in Hep3BCas9 and Hep3BRAB18KO cells pre-treated with or without a non-toxic dose of GCA (50 nM). As predicted, GalNAc-*HPRT1* siRNA generated the strongest target gene silencing in Hep3BRAB18KO cells without GCA treatment (group 3, IC50 = 2.69 nM), and the weakest target gene silencing in Hep3BCas9 cells with GCA treatment (group 2, IC50 N/A) (Figure 5C). Similar levels of *HPRT1* silencing were observed in Hep3BCas9 cells without GCA treatment (group 1, IC50 = 52.31 nM) and Hep3BRAB18KO cells with GCA treatment (group 4, IC50 = 30.40 nM), since only one type of retrograde transport was blocked under these conditions. However, when GalNAc-mediated delivery of GalNAc-*HPRT1* siRNA was replaced with liposome-mediated delivery of unconjugated *HPRT1* siRNA (compound no. 39986), and using otherwise similar experimental conditions to those described above, no difference in the potency of *HPRT1* silencing was observed across groups (Figure 5D). These studies suggest retrograde Golgi-ER transport positively regulates siRNA-mediated gene silencing. However, as demonstrated previously,[1] *RAB18* or retrograde Golgi-ER transport impacts the activity of siRNA delivered by GalNAc but not liposome-mediated transfection.

RAB18 knockout changes siRNA colocalization with LDs

To further elucidate the mechanism by which *RAB18* regulates siRNA trafficking, we conducted imaging-based assays using the anti-siRNA antibody described above to examine siRNA spatial distribution patterns in Hep3BCas9 cells and Hep3BRAB18KO cells. As shown in Figure 6A, the colocalization of siRNA with subcellular structures was visualized using LipidTox to stain for LDs and fluorescent antibodies for AGO2 (Argonaute 2), calreticulum, calnexin, GM130, LAMP2, RAB9, RAB4, and DCP1A (Figures S6 and S7). Hep3BCas9 and Hep3BRAB18KO cells were

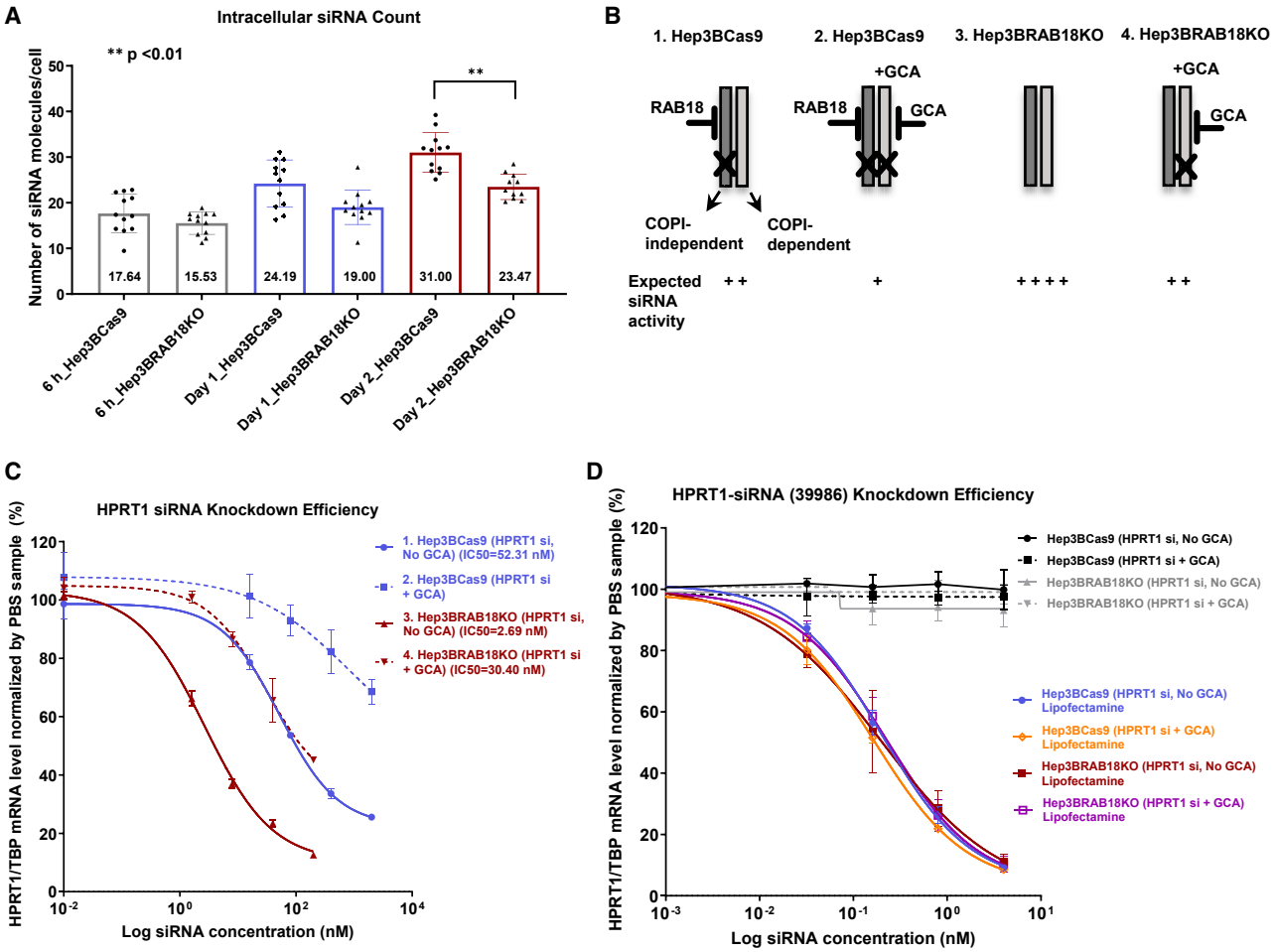

Figure 5. Impact of *RAB18* knockout on intracellular siRNA accumulation and the impact of retrograde Golgi-ER transport on siRNA-mediated gene silencing

(A) Quantification of intracellular siRNA spots measured from imaging at various time points post GalNAc-*HPRT1* siRNA treatment. (B) Schematic diagram of experimental design to evaluate the impact of retrograde Golgi-ER transport on siRNA-mediated gene silencing. (C) dPCR measurements of *HPRT1* expression in Hep3BCas9 or Hep3BRAB18KO cells treated with GalNAc-*HPRT1* siRNA (8172) in the presence or absence of GCA ($n = 3$). (D) dPCR measurements of *HPRT1* expression in Hep3BCas9 or Hep3BRAB18KO cells transfected (Lipofectamine) with unconjugated *HPRT1* siRNA (39986) in the presence or absence of GCA ($n = 3$). The unconjugated *HPRT1* siRNA was directly added to culture medium for groups without Lipofectamine labels. All dPCR samples were measured 4 days post siRNA treatments. All dPCR results shown were normalized by *TBP* and no siRNA (PBS only)-treated control groups. Asterisk indicates significant difference (** $p < 0.01$) based on one-way ANOVA test. All error bars represent SD.

treated with 1.5 μM GalNAc-*HPRT1* siRNA for 1 or 2 days, stained, and then imaged. Since only about 15–30 siRNA spots were detectable per cell (Figure 5A), identifying siRNA colocalization events with any cellular structure was infrequent. To improve identification and quantification, we developed an image-analysis procedure to apply a deep-learning-based approach for cell segmentation (Figure S8) and to calculate the Manders coefficient[16] to indicate siRNA colocalization changes. Of the cell structures examined, the most noteworthy difference was colocalization of siRNA with LDs after 2 days of siRNA treatment (Figures 6B and S9), where a 20% reduction was observed in Hep3BRAB18KO compared to parental cells. To further validate this finding, label-free live-cell holotomographic[17,18] imaging of LDs and siRNA was conducted in Hep3BCas9 and Hep3BRAB18KO cells. As shown in Figure 6C, colocalization analysis on this live-cell imaging revealed a similar reduction of siRNA-LD co-localization in Hep3BRAB18KO cells compared to parental cells after 2 days of siRNA treatment. A reduction of siRNA-LD colocalization might indicate either increased consumption or enhanced degradation of siRNA. The impact of *RAB18* knockout and overexpression on LDs was shown in previous studies. To summarize, overexpression of wild-type (WT) *RAB18* resulted in small, dispersed LDs in WT as well as *RAB18* KO cells.[6,19] *RAB18* KO interferes with LD catabolism, resulting in reduced LD numbers, enlarged LD size, and impaired fatty acid release.[19] To confirm if *RAB18* knockout in Hep3B cells

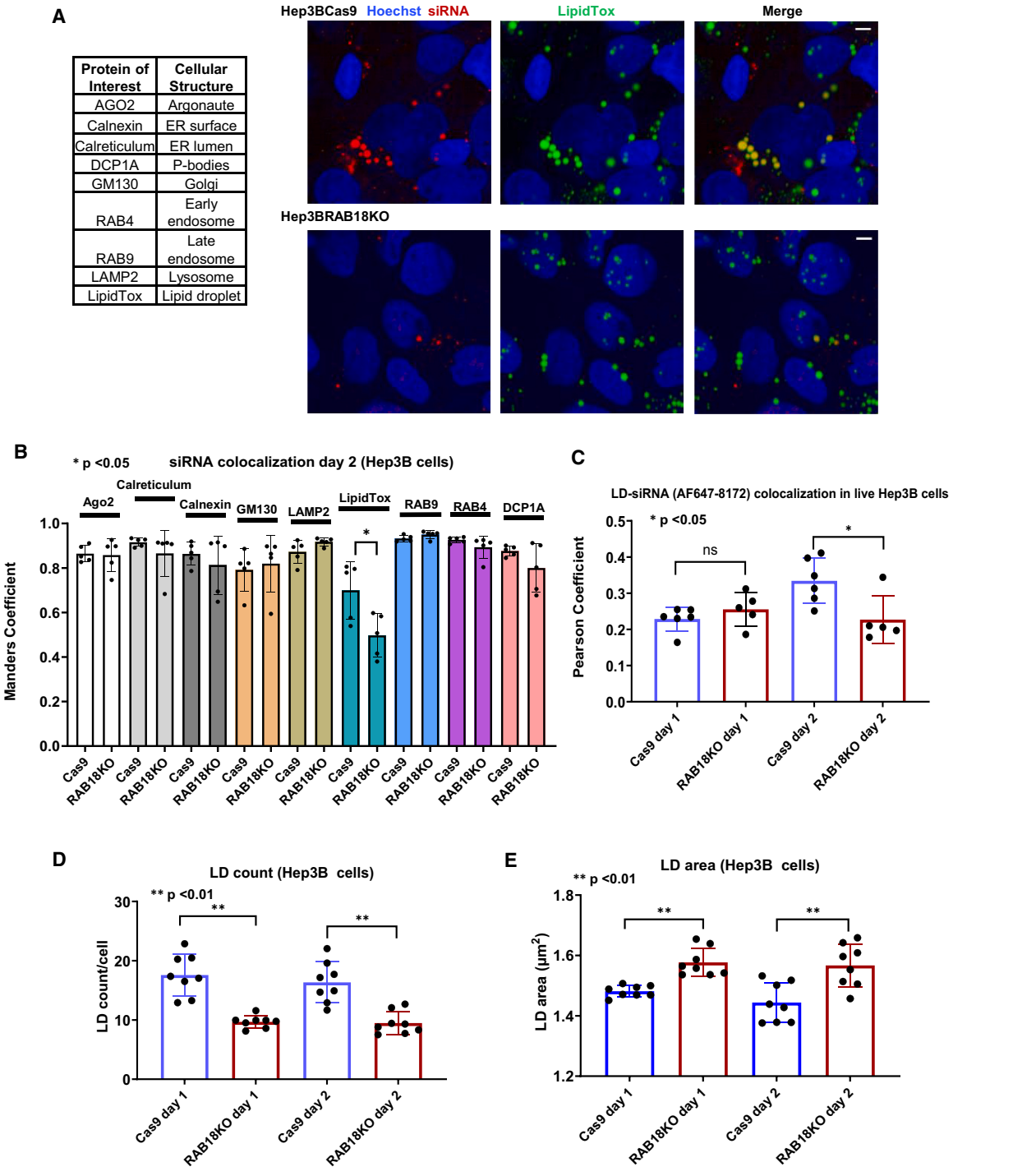

Figure 6. Imaging intracellular siRNA

(A) The table on the left lists the antibodies and corresponding cellular markers evaluated by imaging. On the right, confocal microscopy images show siRNA co-staining with LipidTox (images of the other cellular markers listed are shown in Figures S6 and S7). Scale bars represent 5 μm. (B) Manders coefficient analysis of the images taken from Hep3BCas9 and He3BRAB18KO cells treated with 1.5 μM GalNAc-*HPRT1* siRNA 2 days post siRNA treatment. The Manders coefficient scores reflect the frequency of siRNA colocalization with the given cellular markers. Compared to all other cellular markers, notable siRNA colocalization difference between Hep3BCas9 and

(legend continued on next page)

has the same effect on LDs, the number and size of LDs in Hep3BCas9 and Hep3BRAB18KO cells were quantified. Consistent with previous findings, LDs were both reduced in number and enlarged in size when comparing Hep3BRAB18KO cells to the parental Hep3BCas9 cells (Figures 6D and 6E).

LDs regulate siRNA-mediated gene silencing

The RNA-seq data obtained from the *Rab18* siRNA trigger *in vivo* study demonstrates *Rab18* knockout upregulates genes related to lipid metabolic processes (Figures 3F and 3H), suggesting a role for *RAB18*/*Rab18* in regulating lipid biology. Our imaging study results add to this, showing that *RAB18* expression, or lack thereof, not only changes the number and size of LDs but also impacts siRNA colocalization with LDs (Figures 6B–6E). Therefore, to further elucidate the function of LDs in regulating siRNA-mediated gene silencing, we added oleic acid, a mono-unsaturated omega-9 fatty acid, to culture medium to enhance the intracellular accumulation of LDs[20] or triacsin C, a long fatty acyl-coenzyme A (CoA) synthetase inhibitor to decrease LD content.[20] Hep3BCas9 and Hep3BRAB18KO cells were incubated with non-toxic dosages of oleic acid (100 μM) or triacsin C (1 μM) for 24 h, followed by addition of GalNAc-*HPRT1* siRNA in the presence of oleic acid or triacsin C for 4 days. The effect on target gene *HPRT1* expression was measured across treatment groups and compared with a non-compound-treated negative control through dPCR. Triacsin C treatment in both Hep3BCas9 and Hep3BRAB18KO cells reduced siRNA-mediated silencing of the *HPRT1* gene (Figures 7A and 7B). Conversely, oleic acid treatment in both Hep3BCas9 and Hep3BRAB18KO cells had little or no impact on siRNA-mediated gene silencing of the *HPRT1* gene (Figures 7C and 7D). These results demonstrate that LDs might positively regulate siRNA-mediated gene silencing, and, collectively, our data suggest this is a *RAB18*-mediated mechanism.

RAB18 knockout or knockdown is a prerequisite to enhance siRNA-mediated gene silencing

Herein we have demonstrated that a reduction in *RAB18*, either by gene knockout or siRNA-mediated gene knockdown, enhances siRNA-mediated gene silencing. To further validate if *RAB18* knockout or knockdown is necessary for enhancing siRNA-mediated gene silencing, Hep3BCas9 cells were co-treated with either the same dose of GalNAc-*HPRT1* siRNA and GalNAc-conjugated siRNA targeting *RAB18* (GalNAc-*RAB18* siRNA, compound no. 64131) or the same dose of GalNAc-*HPRT1* siRNA and the control GalNAc-*PPIB* siRNA (Table S1). Compared with Hep3BCas9 cells treated with only GalNAc-*HPRT1* siRNA, co-treatment with either GalNAc-*RAB18* siRNA or GalNAc-*PPIB* siRNA failed to change the silencing potency of GalNAc-*HPRT1* siRNA (Figure 7E). Therefore, to enhance the silencing effect of siRNA conjugates, knockout or knockdown of the *RAB18* gene is required prior to treatment with siRNA conjugates.

DISCUSSION

To reveal the cellular factors limiting delivery of siRNA therapeutics, we performed a genome-wide pooled CRISPR-Cas9 screen based on delivery of GalNAc-conjugated siRNA targeting *HPRT1* in the human hepatocellular carcinoma line Hep3B.[1] Multiple candidate genes, when knocked out, enhanced siRNA efficacy in Hep3B cells. However, by performing a secondary, arrayed CRISPR screen[1] and generating knockout cell lines of a few top candidate genes (data not shown), the most significant enhancement of siRNA-mediated gene silencing was observed in *RAB18* KO cells. As one of the 20 most highly conserved RAB GTPases present in the last eukaryotic common ancestor of both the plant and animal kingdoms,[21,22] the protein encoded by the *RAB18* gene is ubiquitously expressed across a majority of cell and tissue types. The RAB18 protein switches between GDP-bound off and GTP-bound on forms. The active GTP-bound form of RAB18 can recruit different sets of downstream effectors to the plasma membrane to mediate vesicle formation, movement, tethering and fusion,[6,11,23] growth of LDs,[5,6] formation of endoplasmic reticulum-LDs contacts,[23] maintaining endoplasmic reticulum structure,[11] inhibition of COPI-independent retrograde trafficking from Golgi to ER,[7] regulation of secretory granules[8] and peroxisomes,[9] and regulation of apical endocytosis/recycling.[24] RAB18 protein also plays a key role in eye and brain development and neurodegeneration.[25,26]

The transition of RAB18 between the GDP- and GTP-bound conformations is governed by two classes of regulatory proteins: the guanine-nucleotide exchange factors (GEFs), which mediate the exchange of bound GDP for GTP, and the GTPase-activating proteins (GAPs), which stimulate the GTP hydrolysis activity of their substrate GTPase(s). RAB3GAP1 and RAB3GAP2 form complexes with GAP and act as a RAB18 GEF regulator promoting RAB18 activation.[11] The TBC1D20 protein exhibits modest GAP activity toward RAB18 protein and functions to promote RAB18 dissociation from the ER membrane into the cytosol.[27] Loss-of-function mutations in *RAB18*, *RAB3GAP1*, *RAB3GAP2*, and *TBC1D20* have been identified in patients with the human neurological and developmental disorder Warburg micro syndrome, a rare autosomal recessive multisystem disorder primarily characterized by ocular and neurodevelopmental defects.[25–29] *RAB18* activity could also be modulated by regulating *RAB3GAP1*, *RAB3GAP2*, and *TBC1D20* expression. The potential of these genes on directing RAB18 activity is worth exploring in future studies.

Hep3BRAB18KO cells was detected for LipidTox-stained LDs. Each imaging experiment was repeated five times. (C) Pearson coefficient analysis on the refractive and fluorescence images of live Hep3BCas9 and He3BRAB18KO cells treated with 1.5 μM AF647 conjugated GalNAc-*HPRT1* siRNA 1 and 2 days post siRNA treatment. Each imaging experiment was repeated six times. (D) Quantification of LD count on day 1 and day 2 post 1.5 μM GalNAc-*HPRT1* siRNA treatment comparing Hep3BCas9 and Hep3BRAB18KO cells. Each imaging experiment was repeated eight times. (E) Summary of LD size analysis on day 1 or day 2 post 1.5 μM GalNAc-*HPRT1* siRNA treatment comparing Hep3BCas9 and Hep3BRAB18KO cells. Each imaging experiment was repeated eight times. All error bars represent SD. Asterisk indicates significant difference (* $p < 0.05$; ** $p < 0.01$) based on one-way ANOVA test.

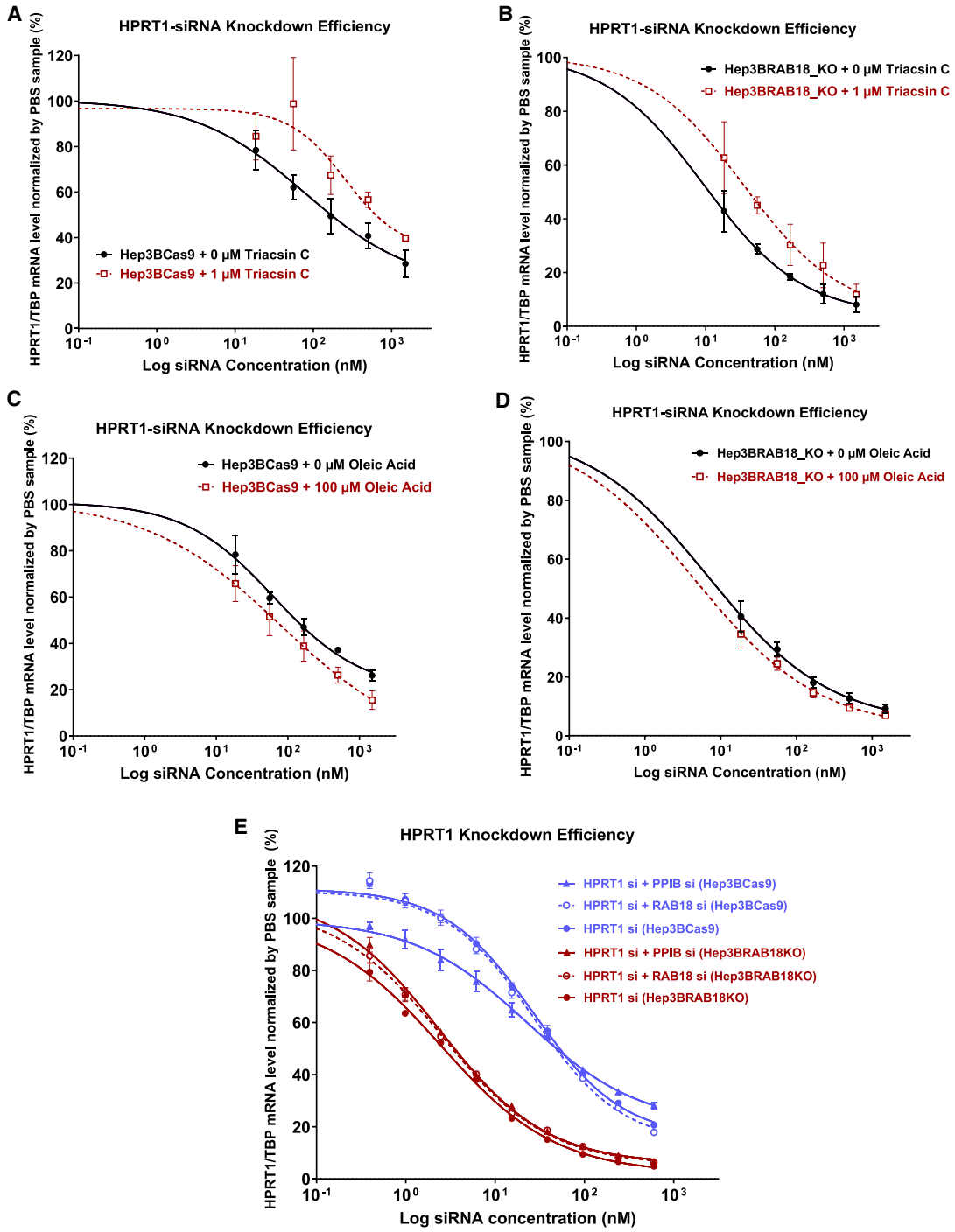

Figure 7. The effects of oleic acid and triacsin C on regulating siRNA-mediated gene silencing and the prerequisite of *RAB18* knockout/knockdown in enhancing siRNA-mediated gene silencing

dPCR measurements of *HPRT1* expression in (A) Hep3BCas9 cells or (B) Hep3BRAB18KO cells treated with GalNAc-*HPRT1* siRNA and triacsin C. Cells were pre-treated with the indicated concentration of triacsin C for 24 h prior to siRNA treatment. dPCR measurements of *HPRT1* expression in (C) Hep3BCas9 cells or (D) Hep3BRAB18KO cells treated with GalNAc-*HPRT1* siRNA and oleic acid. Cells were treated with the indicated concentration of oleic acid for 24 h prior to siRNA treatment. (E) dPCR measurements of *HPRT1* expression in GalNAc-*HPRT1* siRNA-treated Hep3BCas9 and Hep3BRAB18KO cells with or without co-treatment of GalNAc-*RAB18* siRNA or the negative control GalNAc-*PPIB* siRNA. All dPCR samples were measured 4 days post siRNA treatments. All dPCR results shown were normalized by *TBP* and no-siRNA (PBS only)-treated control groups with $n = 3$ for each experiment. All error bars represent SD.

In the study described herein, we show the effect of *RAB18* knockout/knockdown on siRNA-mediated gene silencing recapitulates in both hepatic cells and extrahepatic cells and translates from *in vitro* systems to *in vivo* models. As shown in this study and in previous published work,[1] we observed no growth defect in *RAB18*-knockout Hep3B[1] or T47D cells (Figure S2B). In the current study, *RAB18*/*Rab18* siRNA was conjugated to GalNAc, a sugar molecule that selectively binds a surface protein, ASGPR, primarily expressed on hepatocytes in the liver. GalNAc-mediated delivery of siRNA is a well-established and clinically efficacious means for specifically inhibiting protein translation *in vivo*. Three of the four *Rab18* siRNA triggers had no impact on mouse body weight or liver weight, or serum liver transaminase levels (Figures S3 and S5), nor were there any signs of toxicity in the RNA-seq analysis (Figures 3 and S4). Thus, the deleterious readouts observed with *Rab18* siRNA trigger 64137-1 appear to be trigger specific and not the result of general *Rab18* knockdown (Figures S3B, S3D, and S4E). Furthermore, *Rab18*-deficient mice are reported to be viable and fertile, although they did exhibit major ocular and neurological abnormalities that are associated with Warburg micro syndrome.[13] However, detailed necropsy of *Rab18* KO mice with their littermate controls, including more than 20 tissues across the body, and the brain, showed no substantial differences.[13] Thus, the authors concluded the observed phenotypes in *Rab18* KO mice were not caused by gross disruption of development.[13] Therefore, we deduce it might be achievable to enhance siRNA-mediated gene silencing through transient inhibition of *RAB18* function without causing significant toxicity.

The success of silencing target gene in hepatocytes by siRNA delivered through GalNAc conjugation heavily relies on the cell-type specificity, abundant expression (~500,000 copies per cell),[30] and rapid recycling rate (~15 min) of ASGPR.[31] These factors enable a substantial number of siRNAs to bind and silence target RNA molecules, even when <1% of the siRNAs are estimated to escape from endosomes.[3] It is challenging to find cell-type-specific receptors with properties like ASGPR for extrahepatic cells. However, as well described, RNA silencing is an efficient process once the siRNA is loaded into RISC, and it only requires about 10–110 siRISC (siRNA incorporated into RNA-induced silencing complexe) molecules per cell to achieve approximately 50% silencing of the target gene.[32] Hence, if siRNA could be trafficked into RISC in a more efficient manner, it may be that receptors with sub-optimal qualities would prove sufficient for siRNA delivery and efficacy in extrahepatic cells. As demonstrated in this study, even though *RAB18* knockout reduces the detected amount of intracellular siRNA (Figure 5A), which could indicate increased consumption of siRNA, siRNA-mediated gene silencing is enhanced, suggesting a more organized and efficient intracellular trafficking route for siRNAs in the absence of *RAB18*. To elucidate if *RAB18* knockout changes siRNA intracellular trafficking and its spatial distribution with respect to different subcellular structures, confocal microscopy was used to image multiple intracellular targets, including AGO2, ER surface, ER lumen, P bodies, Golgi, early endosomes, late endosomes, lysosomes, and LDs in both Hep3BCas9 and Hep3BRAB18KO cells (Figures 6, S6, and S7). The only noteworthy result was a 20% reduction of siRNA colocalization with LDs after 2 days of siRNA treatment in Hep3BRAB18KO compared to Hep3BCas9 cells (Figure 6B), implicating the participation of LDs in regulating siRNA activity. Imaging analysis at higher resolution would be needed to evaluate the complex nanoscale interactions of siRNA with specific subcellular structures.

Herein, we have demonstrated that both retrograde Golgi-ER transport and LDs positively regulate siRNA-mediated gene silencing (Figures 5B, 5C, and 7). As rough ER is a central nucleation site of siRNA-mediated gene silencing,[32] it is not surprising to observe retrograde Golgi-ER transport to positively regulate the siRNA-mediated gene silencing. Although *RAB18* mutants have been shown to specifically enhance retrograde Golgi-ER transport of COPI-independent cargo, but not COPI-dependent cargo from the Golgi to ER,[7] more detailed studies would be needed to understand how the *RAB18* gene regulates this process at the molecular level and whether other key genes in retrograde Golgi-ER transport, such as *ARF1*,[33] are involved.

Using triacin C to reduce intracellular LD content, we observed a correlation between siRNA-mediated gene silencing and decreased cellular LD content (Figures 7A and 7B). These results suggest LDs regulate siRNA-mediated silencing efficacy, perhaps through acting as siRNA reservoirs at the end of siRNA trafficking route. Since the number of siRNA molecules deposited into LDs might be pre-determined by multiple upstream trafficking events and independent of the size and number of LDs, simply enhancing LD size and number by oleic acid treatment may not be sufficient to enhance siRNA-mediated gene silencing. Therefore, increasing intracellular LD content with oleic acid had little or no impact on siRNA-mediated gene silencing (Figures 7C and 7D). Genes regulating LD biogenesis or autophagy, such as *DGAT1*,[34] could also regulate LD size. Future studies could include knocking out, or knocking down, such genes to further elucidate the connection between LDs and siRNA activity. LDs are cytosolic lipid storage organelles important for cellular lipid metabolism, energy homeostasis, cell signaling, and inflammation. Lipophagy is a type of autophagy; it is a process by which LDs are degraded in lysosomes. Both starvation and acute lipid stimulus increase autophagic sequestration of LDs and trigger their degradation in lysosomes.[35,36] The *RAB18* gene has been shown to regulate LD metabolism[37] and the formation of ER-LD contacts.[23] As demonstrated in this study and previously[19] (Figures 6D and 6E), there are fewer and larger LDs in *RAB18*-knockout cells. Additionally, knockout of *RAB18* interferes with LD turnover. In WT cells, starvation triggers a time-dependent reduction in LD number and size; this process is repressed in *RAB18*-knockout cells.[19] Hence, if LDs serve as temporal reservoirs for siRNAs, the siRNAs may be degraded when LDs get engulfed by autophagosomes. However, in *RAB18*-knockout cells, lipid metabolism and lipophagy are impaired, causing a low turnaround rate for LDs. This may provisionally protect siRNAs from degradation and provide more opportunities for siRNAs to escape into the cytosol.

The optimal delivery of siRNA into target cells needs to overcome a variety of challenges, including degradation by nucleases, cell

membrane permeability, endosomal escape, and intracellular trafficking. We previously demonstrated that knocking out the *RAB18* has no detectable effect on cell membrane permeability.[1] The studies described herein demonstrate that knocking out *RAB18* enhances siRNA silencing through enhancing siRNA retrograde Golgi-ER transport and positively modulating the LD-mediated regulation of siRNA activities. Therefore, *RAB18* might regulate siRNA silencing by altering intracellular trafficking. The identification and study of factors regulating siRNA degradation, cell membrane permeability, and endosomal escape might elucidate further means to enhance siRNA silencing.

In summary, using a variety of *in vitro* systems, we have demonstrated that knocking out *RAB18* enhances the effect of siRNA-mediated gene silencing in both hepatic and extrahepatic cells. Furthermore, we translated this finding to an *in vivo* model. Altogether, our data point to a mechanism by which *RAB18* regulates the efficacy of siRNA-mediated gene silencing in extrahepatic cells. This role for *RAB18* in RNAi may facilitate the discovery of more cell-type-specific receptors that, in the presence of *RAB18* expression, may be suboptimal for delivering siRNA cargo and achieving efficacious silencing of target genes. Thus, understanding the potential of gene silencing in the presence or absence of concomitant *RAB18* expression may unleash new possibilities in the development of extrahepatic siRNA.

MATERIALS AND METHODS

Cell line and culture condition

Hep3B, T47D, A498, MCF7, and COLO205 cells were purchased from ATCC (https://www.atcc.org/). MiaPaCa-2, HT-29, and NCIH1299 were obtained from the Amgen oncology group at South San Francisco. Hep3B cells were cultured in Eagle's minimum essential medium (ETCC; from ATCC, catalog no. 30-2003) + 10% fetal bovine serum (FBS; HyClone, catalog no. SH30071.03). Hep3Bcas9 cells were cultured in EMEM + 10% FBS + 10 μg/mL blasticidin. Hep3BRAB18KO cells were cultured in EMEM + 10% FBS + 10 μg/mL blasticidin + 0.5 μg/mL puromycin. T47D cells were cultured in Roswell Park Memorial Institute (RPMI; Gibco, catalog no. 11875085) + 10% FBS + 7.4 μg/mL human recombinant insulin (Life Technologies, catalog no. 12585-014). A498 cells were cultured in EMEM + 10% FBS. The culture condition for MCF7 cells is EMEM + 10% FBS + 0.01 mg/mL human recombinant insulin. Both NCIH1299 and COLO205 cells were cultured in RPMI + 10% FBS. HT-29 cells were cultured McCoy's 5A (Gibco, catalog no. 16600108) + 10% FBS. MiaPaCa-2 cells were cultured in Dulbecco's modified Eagle's medium (DMEM; Gibco, catalog no. 11966-025) + 10% FBS + 2.5% horse serum (Cytiva, catalog no. SH30074.04).

In vitro siRNA/ASO treatment, RNA isolation, and dPCR

All *in vitro* siRNA treatments were performed in a 96-well plate format. To deliver GalNAc-siRNA conjugates, GalNAc-ASO conjugates, and the unconjugated siRNA to various cell lines, 50 μL of cell suspension was first added to each well to achieve desired cell densities (Hep3B and its derived cells, 20,000 cells/well; T47D and its derived cells, 20,000 cells/well; A498 and its derived cells, 28,000 cells/well; MCF7 and its derived cells, 13,000 cells/well; COLO205 and its derived cells, 15,000 cells/well; MiaPaCa-2 and its derived cells, 41,000 cells/well; HT-29 and its derived cells, 13,000 cells/well; NCIH1299 and its derived cells, 17,000 cells/well). The siRNA/ASO molecules were then diluted in the corresponding tissue culture medium to twice the desired final concentration. Then 50-μL siRNA/ASO solutions were added to the corresponding wells and co-incubated with cells for 4 days in a 37°C tissue culture incubator before RNA isolation. Total RNA isolation from cells was performed in a 96-well format by using the MagMAX mirVana Total RNA Isolation Kit (Applied Biosystems, catalog no. A27828) and KingFisher Flex automated extraction and purification system (Thermo Fisher Scientific) following the manufacturer's instructions. The cDNAs were then synthesized from total RNA samples using the Applied Biosystems High Capacity cDNA Reverse Transcription kit (catalog no. 4368813) by following the user manual. All dPCR reactions were assembled using a QIAcuity Probe PCR Kit (QIAGEN, catalog no. 250101) as per the user manual. After proper mixing and centrifugation, all dPCR reactions were then transferred to QIAcuity 8.5K 96-well nanoplates (QIAGEN, catalog no. 250021). The nanoplates were then loaded onto the one-place digital PCR instrument QIAcuity Eight (QIAGEN) for performing dPCR. The dPCR copy number readings (copies/20 μL) of both target gene (*HPRT1/Hprt1* or *RAB18/Rab18*) and housekeeping gene *TBP/Tbp* were recorded for each well. The normalized target gene mRNA level was calculated by dividing the dPCR reading of the target gene by the dPCR reading of *TBP/Tbp* taken from the same well. The resulting number of siRNA-treated samples was further divided by the number of no-siRNA-treatment samples to obtain the percentage reading of the target gene mRNA level. The predesigned primer/probe for dPCR assays were obtained from Integrated DNA Technologies with 3.6:1 primer to probe ratio. The assay IDs of primer/probe used for quantifying the human genes are as follows: *HPRT1* Hs.PT.39a.22214821, *RAB18* Hs.PT.58.21332040, and housekeeping *TBP* Hs.PT.58.19489510. The assay IDs of primer/probe used for quantifying the mouse genes are as follows: *Hprt1* Mm.PT.39a.22214828, *Rab18* Mm.PT.58.10341383, and housekeeping *Tbp* Mm.PT.39a.22214839.

RAB18 overexpression

RAB18-overexpression vector (Figure S1A) was synthesized by Azenta Life Sciences and packaged into lentivirus by Cellecta. The lentivirus was then used to transduce Hep3BCas9 and Hep3BRAB18KO cells at multiplicity of infection 1 (MOI_1). The mCherry-positive cells were sorted out twice after transduction to enrich *RAB18*-overexpressed cells.

Generate *RAB18*-knockout cells

To generate T47DRAB18KO cells, a TransEDIT CRISPR Cas9 nuclease expression lentivirus (pCLIP-Cas9-Nuclease-EFS-Blast) ordered from TransOMIC Technologies (catalog no. NC0956087) was simultaneously transduced into Hep3B cells at MOI_1 along with a lentiviral gRNA vector targeting *RAB18* (SIGMA vector: U6-gRNA: PGK-puro-2A-tagBFP, gRNA target sequence: GCTATTATAGAGG

TGCACAGGG) at MOI_10. Three days post transduction, the double-positive transduced T47D cells were then enriched by 10 μg/mL blasticidin + 0.5 μg/mL puromycin for 7 days to get T47DRAB18KO cells. The editing efficacy on the *RAB18* gene was then validated by ICE analysis. *RAB18*-knockout A498, MCF7, COLO205, MiaPaCa-2, HT-29, and NCIH1299 cells were generated by co-electroporating 250 ng of Cas9 Nuclease V3 protein (Integrated DNA Technologies, catalog no. 1081058) and three sgRNAs (100 pmol each) targeting the *RAB18* gene (Table S4) into 50,000 target cells through a Neon Electroporation device (Invitrogen) and a Neon Transfection System 10 μL Kit (Invitrogen, catalog no. MPK1025) following the user manual. Cells were then cultured for 7 days before ICE analysis, western blot analysis, and siRNA treatment.

ICE analysis

Cas9 protein only or Cas9 + *RAB18* sgRNA RNP complex electroporated cells (1×10^6 cells) were harvested by trypsinization, and gDNA was harvested using the DNeasy Blood and Tissue kit (QIAGEN, catalog no. 69504). The *RAB18* exon two genomic locus was amplified from 50 ng of gDNA using forward primer 5′ TTGTTTCTTCCATT TGGATCAG 3′ and reverse primer 5′ TGCCACTATATCCTGTG AGG 3′ and Platinum PCR Supermix High Fidelity (Invitrogen, catalog no. 12532016). The resulting PCR products were Sanger sequenced using primer 5′ ACACAAGGCAACTAGGAACAA 3′ and analyzed for knockout efficacy using the ICE analysis tool (Synthego, https://ice.synthego.com/#/).

RAB18 western blot analysis

Total protein lysate was isolated from Cas9 protein only or Cas9 + *RAB18* sgRNA RNP complex electroporated cells (5×10^6 cells) using RIPA buffer (Thermo Scientific, catalog no. J63306.AK) containing 1× Halt Protease and Phosphatase Inhibitor Cocktail (Thermo Scientific, catalog no. 78440), then clarified by sonication before centrifugation to remove cell debris. Then 50 mg of each protein lysate was size separated on NuPage 4%–12% Bis-Tris gels, then transferred to nitrocellulose membranes and blocked with 3% BSA in 1× TBS-Tween 20 for 1 h at room temperature before probing with rabbit anti-Rab18 (1:1,000, Bioss, catalog no. bsm-51333M) and mouse anti-GAPDH (1:5,000, Cell Signaling Technology, catalog no. 2118S) in 3% BSA-TBS-Tween 20 overnight at 4°C. Membranes were washed three times with 1× TBS-Tween 20, then incubated with IRDye 680RD goat anti-mouse immunoglobulin G (IgG) (1:5,000, Li-cor, catalog no. 926-68070) and IRDye-800CW goat anti-rabbit IgG (1:5,000, Li-cor, catalog no. 926–32211) in 5% nonfat dry milk in TBS-Tween 20 for 1 h at room temperature. Membranes were washed three times with 1× TBS-Tween 20 and then imaged on a Li-cor Odyssey 9120 imager.

Human iPSC-derived cardiomyocyte culture for *RAB18* siRNA knockdown study

iCell Cardiomyocytes[2] were thawed according to the manufacturer's instructions (FUJIFILM Cellular Dynamics, catalog no. R1017) directly onto fibronectin (Stem Cell Technologies, catalog no. 07159) and gelatin (Stem Cell Technologies, catalog no. 07903)-coated 96-well plates at a density of 50,000 cells per well. Four hours later, the medium was switched to CDI maintenance medium (FUJIFILM Cellular Dynamics, catalog no. M1003). iCell Cardiomyocytes[2] were fed with fresh CDI maintenance medium every 2 days. On day two, iCell Cardiomyocytes[2] were transfected with either NT siRNA or *RAB18* siRNA at the final concentration of 10 nM using Lipofectamine RNAiMAX Transfection Reagent (Invitrogen, catalog no. 13778075) following the manufacturer's instructions. The medium was switched to fresh CDI maintenance medium 24 h later. On days 5 and 7, either NT siRNA or *HPRT1* siRNA at 2 μM were diluted in fresh CDI maintenance medium and added to iCell Cardiomyocytes[2] culture. On day 9, the cells were collected for RNA extraction.

Animals

All animal procedures described herein were approved by the Institutional Animal Care and Use Committee (IACUC) of Charles River Accelerator and Development Lab (CRADL, AAALAC accredited) and cared for in accordance with the Guide for the Care and Use of Laboratory Animals, Eighth Edition (National Research Council, US). Mice were group housed in a climate-controlled room at 22°C ± 2°C with a 12-h light, 12-h darkness cycle (0600–1800 h). Animals had *ad libitum* access to a regular chow diet (Envigo, catalog no. 2920X) and were caged in irradiated Innovive Disposable IVC Rodent Caging Systems (San Diego, CA) with pre-filled sterile and acidified water bottles. Eight- to 10-week-old, pathogen-free female C57BL/6 mice (Charles River Laboratories) were used for all *in vivo* studies.

In vivo studies

Prior to study initiation, mouse body weights were collected, randomized by weight, and then sorted into experimental groups. At study initiation, mice received a subcutaneous injection of siRNA into the left abdomen region; all siRNAs (0.5 mmol/L) were diluted in Dulbecco's Phosphate Buffered Saline (DPBS; Thermo Fisher Scientific, catalog no. 14190-136) to a concentration of 0.5, 1, or 3 mg/kg of animal, and adjusted to a volume of 160 μL per animal. Control vehicle groups were administered equal volumes of DPBS. Mice were harvested after 14 days or as indicated in the corresponding figures, reinjected with another round of siRNA or vehicle, and then harvested 14 days after the second dose. siRNAs are listed and detailed in Table S1.

At study termination, mice were weighed and then anesthetized with isoflurane. From each animal, blood was collected via intracardiac puncture using a 1-mL 25-gauge Tuberculin syringe and transferred to Microtainer SST tube (Molecular Devices, catalog no. 365967). Mice, still under deep anesthesia, were then euthanized by a secondary physical method and the whole liver was collected and weighed; the left lobe was immediately snap-frozen in liquid nitrogen for mRNA isolation and analysis. Filled SST tubes stood at room temperature to clot for a minimum of 30 min and then spun, at room temperature, for 5 min at 10,000 rpm in a centrifuge. Serum was then transferred to a 96-well DeepWell plate (Axygen, catalog no. P-2ML-SQ-C), sealed, frozen, and stored at −80°C.

Serum analysis

Frozen serum was sent to IDEXX BioAnalytics (West Sacramento, CA) for determination of the following clinical chemistry endpoints: alanine aminotransferase (ALT), aspartate aminotransferase (AST), and alkaline phosphatase (ALP). All data reported in this manuscript came directly from the IDEXX report.

RNA isolation and analysis

For the *in vivo* study, total RNA samples were isolated from frozen liver samples by using a RNeasy Mini Kit (QIAGEN, catalog no. 74104). The concentration and quality of the isolated RNA samples were assessed and determined on Agilent 4200 TapeStation system and had RNA integrity numbers more than 8.6. Total RNA (500 ng) was used to prepare a cDNA library by using a protocol modified from the Illumina TruSeq Stranded mRNA kit (Illumina, catalog no. 20020595). Briefly, after poly(A) + RNA selection, fragmentation, and priming, the fragmented RNA was transcribed to cDNA in the reaction of reverse transcription containing SuperScript III (Thermo Fisher Scientific- Invitrogen, catalog no. 18080093) and, sequentially, the products of the first-strand cDNA synthesis reaction were converted to double- stranded cDNAs and subjected to end-repair, A-tailing, and adapter ligation by following the commercial instructions. The dUTP-containing strands were destroyed by digestion with USER enzymes (New England Biolabs). The constructed libraries were amplified using the PCR program: a denaturation step at 98°C for 30 s, 15 cycles of 95°C for 10 s, 60°C for 30 s, 72°C for 30 s, and a 72°C extension cycle for 5 min followed by a hold step at 4°C. Libraries were sequenced to a minimum depth of 35 million paired-end reads on an Illumina NovaSeq6000 with the 100- or 150-nt read length. The RNA-seq reads were aligned using the OSA (Omicsoft Studio Aligner) aligner integrated into Omicsoft Studio (v10; QIAGEN), using the human genome version GRCh38 and the GENCODE v24 gene model. Raw gene-level quantification was performed based on the Omicsoft implementation of RSEM (RNA-Seq by Expectation Maximization). Differential expression analysis was performed using DESeq2.[38] For the comparative analysis, genes with an average normalized count less than 50 in both conditions were excluded. Gene Ontology (GO) pathway enrichment was tested using enrichR.[39] In short, enrichR uses Fischer's exact test to calculate *p* value to determine if a list of input genes significantly overlaps with an annotated gene set. The adjusted *p* value is calculated using the Benjamini-Hochberg method.

Immunofluorescence and imaging

Antibodies used in imaging experiments include AGO2 (1:50, Abcam, catalog no. Ab57113), calreticulum (1:200, Novus Biologicals, catalog no. NBP1-47518SS), calnexin (1:50, Thermo Fisher, catalog no. MA3-027), GM130 (1:200 BD Biosciences, catalog no. 610822), LAMP1 (1:100 Abcam, catalog no. ab25631), LAMP2 (1:100 Abcam, catalog no. ab25631), RAB9 (1:100, Thermo Fisher, catalog no. MA3-067), RAB4 (1:1000, Thermo Fisher, catalog no. MA5-17161), and DCP1A (1:100, Sigma Aldrich, catalog no. WH0055802M6). An in-house-developed rabbit polyclonal anti-siRNA antibody recognizing 2′OMe- and 2′F-containing oligonucleotides was used to stain siRNA molecules.

Dissociated Hep3B and Hep3BRAB18KO cells from culture were seeded onto 96-well PhenoPlate microplates (PerkinElmer) with siRNA and incubated for different time points: 6 h, 1 day, and 2 days. Cell seeding density was adjusted for incubation times. Cells were rinsed once with PBS and fixed with 4% paraformaldehyde (PFA) for 10 min at room temperature and washed twice in PBS for 5 min each. Cells were then permeabilized in PBS with 0.1% Triton X-100 for 25 min and rinsed in PBS twice. Cells were then blocked with 2% BSA for 30 min, rinsed three times, and incubated with primary antibodies and DRAQ5 (Thermo Scientific, catalog no. PI62251) at appropriate concentrations overnight at 4°C. The following day, cells were washed three times in PBS for 5 min each. Fluorescent secondary antibodies (1:200, Thermo Fisher, Alexa Fluor 405/488, catalog no. A31556/catalog no. A11001) were added for 1 h at room temperature and washed three times in PBS. Cells were stained for lipid bodies with LipidTox (1:1,000, Thermo Fisher, catalog no. H34475) and subsequently washed once with PBS and placed in a final solution of PBS. Confocal microscopy images were captured on an Opera Phenix High Content Screening system (PerkinElmer) via a spinning disk confocal at 63× objective magnification to provide a pixel size of ∼160 nm with z stack acquisition where desired.

Image analysis

The Columbus high-volume image data storage and analysis system (v2.9) was used to configure a cell and spot segmentation and analysis sequence. This procedure is typically *ad hoc*, with the user being responsible for organizing a set of sequential "building blocks" to create a sample-specific image-processing pipeline. The following analysis sequence was used quantify and characterize siRNA and LDs.

Input image

View original images from selected data.

Find cells

Cellular area, splitting sensitivity, and common threshold parameters are tested and set manually based on cell type.

Select population

Remove all segmented cells in contact with the image border. Filter out erroneously segmented objects and cells, including cell debris and background, based on object roundness and area parameter thresholds.

Find spots

Find spots that are indicative of siRNA or LDs.

Calculate morphology properties

Collect roundness and area parameters for all selected cells and LDs.

Calculate properties

Quantify cell, LD, and siRNA fluorescent signal.

Define results

Average and collect final cell counts, LD counts, area and morphology, and siRNA total counts and counts per cell.

Colocalization image analysis was performed via Acapella software (PerkinElmer). Briefly, the DRAQ5 channel was used for nuclear and cytoplasmic segmentation. Colocalization was measured in the cytoplasmic region between siRNA and a specific cellular marker using the Manders overlap coefficient.[16] The Manders coefficient was applied for its biological significance as a direct measure of co-occurrence, independent of signal proportionality. In the cases where Acapella provided inaccurate or incomplete cell segmentation, a custom colocalization analysis sequence was prepared in Python v3 to apply Cellpose 2.0.[40] Cellpose deep-learning segmentation models were trained to readily accommodate limited cytoplasmic fluorescence from DRAQ5 and to enable consistent cell segmentation across the different localization patterns observed for the various cellular targets (AF488 staining). Cellpose training parameters, plots of the training loss across iterative rounds of training/image annotation, and example segmentation results are provided in Figure S8. Cell and siRNA spot segmentation masks were applied to the image data and Manders colocalization coefficients were calculated.

Live-cell holotomography

Label-free live-cell holotomography was performed on LDs and siRNA in Hep3B cells. Holotomographic microscopy is a label-free microscopic method used to determine the refractive indices of cells in three dimensions at high spatial and temporal resolution without phototoxicity. The characteristic refractive index of LDs clearly enables their segmentation from the remainder of the cell.[17,18] Label-free imaging of live Hep3B cells was performed as previously described.[17] Briefly, Hep3BCas9 and Hep3BRAB18KO cells were seeded onto 96-well glass-bottom plates (MatTek Corporation) (10,000–12,000 cells per 90 μL of phenol red-free EMEM medium; Quality Biological) with vehicle, 1.5 μM GalNAc-HPRT siRNA (8172), or 1.5 μM AF647 conjugated GalNAc-HPRT siRNA and incubated in tissue culture incubator supplied with 5% CO_2 for 1 or 2 days. Prior to imaging at each time point, cells were rinsed and exchanged with 85 μL of phenol red-free medium. The plate was briefly centrifuged to prevent meniscus formation and loaded on the pre-equilibrated (37°C, 5% CO_2/95% hydrated air) Nanolive CX-A 3D Cell Explorer microscope equipped with class 1 low-power laser (λ = 520 nm, sample exposure 2 mW/mm^2) and 60× magnification air objective (NA 0.8/WD 0.3 mm) (Nanolive, Tolochenaz, Switzerland). After 1 h of plate thermalization, refractive index and fluorescence images (CY5 channel) were acquired using the 3 × 3 GridScan mode (a field view of 236 × 236 μm). For LD characterization, cells and LDs in refractive images were segmented and quantified using the Smart Lipid Droplet Assay module (version 2.0) in the AI/ML (Artificial Intelligence/Machine Learning)-powered Nanolive.[17,18] For colocalization measurement between AF647 conjugated GalNAc-HPRT siRNA and LDs, refractive and fluorescence images were imported into Huygens Professional software (version 22.10) (Scientific Volume Imaging, Hilversum, the Netherlands). Colocalization analysis was performed with Huygens Colocalization Analyzer module using Gaussian minimum threshold estimation and the Pearson coefficient was used to measure the colocalization between AF647 conjugated GalNAc-HPRT siRNA and LDs.

GCA treatment

The toxicity of GCA (Sigma Aldrich, catalog no. 345862-10MG) on cell viability was first evaluated by treating 20,000 Hep3BCas9 cells with 25, 50, 100, and 200 nM GCA for 3 days in a 96-well plate format. Characterized as the highest non-toxic concentration (data not shown), 50 nM GCA was then used for subsequent studies. To validate the impact of GCA treatment on siRNA-mediated gene silencing, 10,000 Hep3BCas9 or Hep3BRAB18KO cells were seeded together with 50 nM GCA in a 96-well plate for 24 h. Medium was then removed from the plate, fresh medium contained the desired concentration of siRNA, and 50 nM GCA was added to each well as describe above in the section "*in vitro* siRNA/ASO treatment, RNA isolation, and dPCR." Two days post siRNA treatment, to ensure the constitutive function of GCA, without removing medium from the plate, 1 μL of 5 μM GCA solution was added to each well and mixed well. The plate was then incubated for another 2 days before RNA isolation, cDNA synthesis, and dPCR assay.

Oleic acid and triacsin C treatment

The toxicity of oleic acid (Sigma Aldrich, catalog no. O1008-5G) and triacsin C (Sigma Aldrich, catalog no. T4540-1MG) on cell viability was first evaluated by treating 20,000 Hep3BCas9 cells with 20, 100, and 200 μM oleic acid or 0.2, 1, and 2 μM triacsin C for 3 days in a 96-well plate format. However, 200 μM oleic acid and 2 μM triacsin C led to toxicity (data not shown) and 20 μM oleic acid and 0.2 μM triacsin C had no obvious effect. Thus, 100 μM oleic acid and 1 μM triacsin C were used for the following studies. To validate the impact of oleic acid and triacsin C treatment on siRNA-mediated gene silencing, 10,000 Hep3BCas9 or Hep3BRAB18KO cells were seeded together with 100 μM oleic acid or 1 μM triacsin C in a 96-well plate for 24 h. Medium was then removed from the plate, and then fresh medium containing the desired concentration of siRNA and the same dosage of oleic acid or triacsin C was added back to the plate. The plate was then incubated for another 4 days before RNA isolation, cDNA synthesis, and dPCR assay.

Notification

Except the *in vivo* studies and the related RNA-seq studies, all other experiments described in the manuscript were repeated more than twice.

DATA AND CODE AVAILABILITY

The row data required to reproduce the above findings are available from the corresponding authors upon request.

ACKNOWLEDGMENTS

This work was totally supported by the Amgen South San Francisco site Precision Biology group.

AUTHOR CONTRIBUTIONS

J. Lu and S.W. conceived and designed the study. J. Lu carried out the ASO studies in Hep3BCas9 and Hep3BRAB18KO cells; performed siRNA studies in *RAB18*-overexpression cell lines; generated *RAB18*-knockout MiaPaCa-2, A498, NCIH1299, COLO25, HT-29, and MCF7 cells and conducted siRNA studies in these extrahepatic cells; performed RNA extraction and dPCR analysis of the *in vivo* study samples and the siRNA-treated human iPSC-derived cardiomyocytes; executed studies that elucidated that retrograde transport positively regulates siRNA-mediated gene silencing; and drafted the manuscript. J. Lee generated T47DCas9 and T47DRAB18KO cells and conducted siRNA efficacy tests in these cells; performed high-content confocal immunofluorescence imaging studies and reproduced the siRNA studies in *RAB18*-knockout MiaPaCa-2, A498, NCIH1299, COLO25, HT-29, and MCF7 cells. E.Y. generated *RAB18*-overexpression cell lines and reproduced the siRNA studies in *RAB18*-knockout MiaPaCa-2, A498, NCIH1299, COLO25, HT-29, and MCF7 cells. D.L.W. developed the method to analyze high-content confocal immunofluorescence imaging results. M.K. conducted RNA-seq data analysis to assess the impact of knocking down *RAB18* in mouse liver. D.P., J.B., and I.C.R. designed and conducted animal work. J.X. and J.F. designed and performed live-cell holotomography studies. J. Long, B.M., and B.W. conjugated siRNA molecules evaluated in this study. O.H. provided statistic support to design siRNA triggers targeting the *RAB18* gene and validated the off-target potential of these triggers. T.G. performed RNA extraction and dPCR analysis of the first-round *in vivo* study samples. W.G. and J.C. performed siRNA treatment in human iPSC-derived cardiomyocytes. H.Z. prepared RNA libraries of the *in vivo* samples for RNA-seq studies. I.C.R., D.L.W., M.K., E.Y., and J. Lee provided constructive comments and suggestions on drafting the manuscript. All authors approved the final version of the manuscript and agree to be held accountable for the content therein.

DECLARATION OF INTERESTS

J. Lu, J. Lee, E.Y., D.L.W., M.K., D.P., J.B., I.C.R., J.X., J.F., J. Long, B.M., O.H., W.G., T.G., H.Z., B.W., J.C., and S.W. are employees at Amgen Inc. All authors owned Amgen shares when the study was conducted. However, these do not alter the authors' adherence to all journal policies on sharing data and materials. None of the authors serve as a current editorial team member for this journal. A patent application entitled "compositions and methods for enhancing gene silencing activity of oligonucleotide compounds" has been filed (WO2023059629A1 WIPO (PCT)).

SUPPLEMENTAL INFORMATION

Supplemental information can be found online at https://doi.org/10.1016/j.omtn.2024.102335.

REFERENCES

1. Lu, J., Swearingen, E., Hardy, M., Collins, P., Wu, B., Yuan, E., Lu, D., Li, C.M., Wang, S., and Ollmann, M. (2022). RAB18 is a key regulator of GalNAc-conjugated siRNA-induced silencing in Hep3B cells. Mol. Ther. Nucleic Acids *28*, 423–434. https://doi.org/10.1016/j.omtn.2022.04.003.
2. Prakash, T.P., Graham, M.J., Yu, J., Carty, R., Low, A., Chappell, A., Schmidt, K., Zhao, C., Aghajan, M., Murray, H.F., et al. (2014). Targeted delivery of antisense oligonucleotides to hepatocytes using triantennary N-acetyl galactosamine improves potency 10-fold in mice. Nucleic Acids Res. *42*, 8796–8807. https://doi.org/10.1093/nar/gku531.
3. Gilleron, J., Querbes, W., Zeigerer, A., Borodovsky, A., Marsico, G., Schubert, U., Manygoats, K., Seifert, S., Andree, C., Stöter, M., et al. (2013). Image-based analysis of lipid nanoparticle-mediated siRNA delivery, intracellular trafficking and endosomal escape. Nat. Biotechnol. *31*, 638–646. https://doi.org/10.1038/nbt.2612.
4. Cardarelli, F., Digiacomo, L., Marchini, C., Amici, A., Salomone, F., Fiume, G., Rossetta, A., Gratton, E., Pozzi, D., and Caracciolo, G. (2016). The intracellular trafficking mechanism of Lipofectamine-based transfection reagents and its implication for gene delivery. Sci. Rep. *6*, 25879. https://doi.org/10.1038/srep25879.
5. Martin, S., Driessen, K., Nixon, S.J., Zerial, M., and Parton, R.G. (2005). Regulated localization of Rab18 to lipid droplets: effects of lipolytic stimulation and inhibition of lipid droplet catabolism. J. Biol. Chem. *280*, 42325–42335. https://doi.org/10.1074/jbc.M506651200.
6. Xu, D., Li, Y., Wu, L., Li, Y., Zhao, D., Yu, J., Huang, T., Ferguson, C., Parton, R.G., Yang, H., and Li, P. (2018). Rab18 promotes lipid droplet (LD) growth by tethering the ER to LDs through SNARE and NRZ interactions. J. Cell Biol. *217*, 975–995. https://doi.org/10.1083/jcb.201704184.
7. Dejgaard, S.Y., Murshid, A., Erman, A., Kizilay, O., Verbich, D., Lodge, R., Dejgaard, K., Ly-Hartig, T.B.N., Pepperkok, R., Simpson, J.C., and Presley, J.F. (2008). Rab18 and Rab43 have key roles in ER-Golgi trafficking. J. Cell Sci. *121*, 2768–2781. https://doi.org/10.1242/jcs.021808.
8. Vazquez-Martinez, R., Cruz-Garcia, D., Duran-Prado, M., Peinado, J.R., Castaño, J.P., and Malagon, M.M. (2007). Rab18 inhibits secretory activity in neuroendocrine cells by interacting with secretory granules. Traffic *8*, 867–882. https://doi.org/10.1111/j.1600-0854.2007.00570.x.
9. Gronemeyer, T., Wiese, S., Grinhagens, S., Schollenberger, L., Satyagraha, A., Huber, L.A., Meyer, H.E., Warscheid, B., and Just, W.W. (2013). Localization of Rab proteins to peroxisomes: a proteomics and immunofluorescence study. FEBS Lett. *587*, 328–338. https://doi.org/10.1016/j.febslet.2012.12.025.
10. Salloum, S., Wang, H., Ferguson, C., Parton, R.G., and Tai, A.W. (2013). Rab18 binds to hepatitis C virus NS5A and promotes interaction between sites of viral replication and lipid droplets. PLoS Pathog. *9*, e1003513. https://doi.org/10.1371/journal.ppat.1003513.
11. Gerondopoulos, A., Bastos, R.N., Yoshimura, S.I., Anderson, R., Carpanini, S., Aligianis, I., Handley, M.T., and Barr, F.A. (2014). Rab18 and a Rab18 GEF complex are required for normal ER structure. J. Cell Biol. *205*, 707–720. https://doi.org/10.1083/jcb.201403026.
12. Gruber, J., Boese, G., Tuschl, T., Osborn, M., and Weber, K. (2004). RNA interference by osmotic lysis of pinosomes: liposome-independent transfection of siRNAs into mammalian cells. Biotechniques *37*, 96–102. https://doi.org/10.2144/04371RR01.
13. Carpanini, S.M., McKie, L., Thomson, D., Wright, A.K., Gordon, S.L., Roche, S.L., Handley, M.T., Morrison, H., Brownstein, D., Wishart, T.M., et al. (2014). A novel mouse model of Warburg Micro syndrome reveals roles for RAB18 in eye development and organisation of the neuronal cytoskeleton. Dis. Model. Mech. *7*, 711–722. https://doi.org/10.1242/dmm.015222.
14. Saenz, J.B., Sun, W.J., Chang, J.W., Li, J., Bursulaya, B., Gray, N.S., and Haslam, D.B. (2009). Golgicide A reveals essential roles for GBF1 in Golgi assembly and function. Nat. Chem. Biol. *5*, 157–165. https://doi.org/10.1038/nchembio.144.
15. Qiu, C., Han, H.H., Sun, J., Zhang, H.T., Wei, W., Cui, S.H., Chen, X., Wang, J.C., and Zhang, Q. (2019). Regulating intracellular fate of siRNA by endoplasmic reticulum membrane-decorated hybrid nanoplexes. Nat. Commun. *10*, 2702. https://doi.org/10.1038/s41467-019-10562-w.
16. Manders, E.M.M., Verbeek, F.J., and Aten, J.A. (1993). Measurement of co-localization of objects in dual-colour confocal images. J. Microsc. *169*, 375–382. https://doi.org/10.1111/j.1365-2818.1993.tb03313.x.
17. Sherman, D.J., Liu, L., Mamrosh, J.L., Xie, J., Ferbas, J., Lomenick, B., Ladinsky, M.S., Verma, R., Rulifson, I.C., and Deshaies, R.J. (2023). The fatty liver disease-causing protein PNPLA3-I148M alters lipid droplet-Golgi dynamics. Preprint at bioRxiv. https://doi.org/10.1101/2023.10.13.562302.
18. Sandoz, P.A., Tremblay, C., van der Goot, F.G., and Frechin, M. (2019). Image-based analysis of living mammalian cells using label-free 3D refractive index maps reveals new organelle dynamics and dry mass flux. PLoS Biol. *17*, e3000553. https://doi.org/10.1371/journal.pbio.3000553.
19. Bekbulat, F., Schmitt, D., Feldmann, A., Huesmann, H., Eimer, S., Juretschke, T., Beli, P., Behl, C., and Kern, A. (2020). RAB18 Loss Interferes With Lipid Droplet Catabolism and Provokes Autophagy Network Adaptations. J. Mol. Biol. *432*, 1216–1234. https://doi.org/10.1016/j.jmb.2019.12.031.
20. Fujimoto, Y., Itabe, H., Kinoshita, T., Homma, K.J., Onoduka, J., Mori, M., Yamaguchi, S., Makita, M., Higashi, Y., Yamashita, A., and Takano, T. (2007). Involvement of ACSL in local synthesis of neutral lipids in cytoplasmic lipid droplets in human hepatocyte HuH7. J. Lipid Res. *48*, 1280–1292. https://doi.org/10.1194/jlr.M700050-JLR200.
21. Elias, M., Brighouse, A., Gabernet-Castello, C., Field, M.C., and Dacks, J.B. (2012). Sculpting the endomembrane system in deep time: high resolution phylogenetics of Rab GTPases. J. Cell Sci. *125*, 2500–2508. https://doi.org/10.1242/jcs.101378.
22. Klopper, T.H., Kienle, N., Fasshauer, D., and Munro, S. (2012). Untangling the evolution of Rab G proteins: implications of a comprehensive genomic analysis. BMC Biol. *10*, 71. https://doi.org/10.1186/1741-7007-10-71.

23. Li, D., Zhao, Y.G., Li, D., Zhao, H., Huang, J., Miao, G., Feng, D., Liu, P., Li, D., and Zhang, H. (2019). The ER-Localized Protein DFCP1 Modulates ER-Lipid Droplet Contact Formation. Cell Rep. *27*, 343–358.e5. https://doi.org/10.1016/j.celrep.2019.03.025.

24. Lutcke, A., Parton, R.G., Murphy, C., Olkkonen, V.M., Dupree, P., Valencia, A., Simons, K., and Zerial, M. (1994). Cloning and subcellular localization of novel rab proteins reveals polarized and cell type-specific expression. J. Cell Sci. *107*, 3437–3448. https://doi.org/10.1242/jcs.107.12.3437.

25. Bem, D., Yoshimura, S.I., Nunes-Bastos, R., Bond, F.C., Kurian, M.A., Rahman, F., Handley, M.T.W., Hadzhiev, Y., Masood, I., Straatman-Iwanowska, A.A., et al. (2011). Loss-of-function mutations in RAB18 cause Warburg micro syndrome. Am. J. Hum. Genet. *88*, 499–507. https://doi.org/10.1016/j.ajhg.2011.03.012.

26. Wu, Q., Sun, X., Yue, W., Lu, T., Ruan, Y., Chen, T., and Zhang, D. (2016). RAB18, a protein associated with Warburg Micro syndrome, controls neuronal migration in the developing cerebral cortex. Mol. Brain *9*, 19. https://doi.org/10.1186/s13041-016-0198-2.

27. Handley, M.T., Carpanini, S.M., Mali, G.R., Sidjanin, D.J., Aligianis, I.A., Jackson, I.J., and FitzPatrick, D.R. (2015). Warburg Micro syndrome is caused by RAB18 deficiency or dysregulation. Open Biol. *5*, 150047. https://doi.org/10.1098/rsob.150047.

28. Aligianis, I.A., Morgan, N.V., Mione, M., Johnson, C.A., Rosser, E., Hennekam, R.C., Adams, G., Trembath, R.C., Pilz, D.T., Stoodley, N., et al. (2006). Mutation in Rab3 GTPase-activating protein (RAB3GAP) noncatalytic subunit in a kindred with Martsolf syndrome. Am. J. Hum. Genet. *78*, 702–707. https://doi.org/10.1086/502681.

29. Aligianis, I.A., Johnson, C.A., Gissen, P., Chen, D., Hampshire, D., Hoffmann, K., Maina, E.N., Morgan, N.V., Tee, L., Morton, J., et al. (2005). Mutations of the catalytic subunit of RAB3GAP cause Warburg Micro syndrome. Nat. Genet. *37*, 221–223. https://doi.org/10.1038/ng1517.

30. Spiess, M. (1990). The asialoglycoprotein receptor: a model for endocytic transport receptors. Biochemistry *29*, 10009–10018. https://doi.org/10.1021/bi00495a001.

31. Schwartz, A.L., Fridovich, S.E., and Lodish, H.F. (1982). Kinetics of internalization and recycling of the asialoglycoprotein receptor in a hepatoma cell line. J. Biol. Chem. *257*, 4230–4237.

32. Stalder, L., Heusermann, W., Sokol, L., Trojer, D., Wirz, J., Hean, J., Fritzsche, A., Aeschimann, F., Pfanzagl, V., Basselet, P., et al. (2013). The rough endoplasmatic reticulum is a central nucleation site of siRNA-mediated RNA silencing. EMBO J. *32*, 1115–1127. https://doi.org/10.1038/emboj.2013.52.

33. Rothman, J.E., and Wieland, F.T. (1996). Protein sorting by transport vesicles. Science *272*, 227–234. https://doi.org/10.1126/science.272.5259.227.

34. Nguyen, T.B., Louie, S.M., Daniele, J.R., Tran, Q., Dillin, A., Zoncu, R., Nomura, D.K., and Olzmann, J.A. (2017). DGAT1-Dependent Lipid Droplet Biogenesis Protects Mitochondrial Function during Starvation-Induced Autophagy. Dev. Cell *42*, 9–21.e5. https://doi.org/10.1016/j.devcel.2017.06.003.

35. Martinez-Lopez, N., and Singh, R. (2015). Autophagy and Lipid Droplets in the Liver. Annu. Rev. Nutr. *35*, 215–237. https://doi.org/10.1146/annurev-nutr-071813-105336.

36. Chandak, P.G., Radovic, B., Aflaki, E., Kolb, D., Buchebner, M., Fröhlich, E., Magnes, C., Sinner, F., Haemmerle, G., Zechner, R., et al. (2010). Efficient phagocytosis requires triacylglycerol hydrolysis by adipose triglyceride lipase. J. Biol. Chem. *285*, 20192–20201. https://doi.org/10.1074/jbc.M110.107854.

37. Li, C., Luo, X., Zhao, S., Siu, G.K., Liang, Y., Chan, H.C., Satoh, A., and Yu, S.S. (2017). COPI-TRAPPII activates Rab18 and regulates its lipid droplet association. EMBO J. *36*, 441–457. https://doi.org/10.15252/embj.201694866.

38. Love, M.I., Huber, W., and Anders, S. (2014). Moderated estimation of fold change and dispersion for RNA-seq data with DESeq2. Genome Biol. *15*, 550. https://doi.org/10.1186/s13059-014-0550-8.

39. Xie, Z., Bailey, A., Kuleshov, M.V., Clarke, D.J.B., Evangelista, J.E., Jenkins, S.L., Lachmann, A., Wojciechowicz, M.L., Kropiwnicki, E., Jagodnik, K.M., et al. (2021). Gene Set Knowledge Discovery with Enrichr. Curr. Protoc. *1*, e90. https://doi.org/10.1002/cpz1.90.

40. Pachitariu, M., and Stringer, C. (2022). Cellpose 2.0: how to train your own model. Nat. Methods *19*, 1634–1641. https://doi.org/10.1038/s41592-022-01663-4.